Stiffness characteristics of composite beams and application in damage identification

Citation for published version:
Gu, Y & Lu, Y 2023, 'Stiffness characteristics of composite beams and application in damage identification', *Journal of Engineering Mechanics*, vol. 149, no. 9, 04023063. https://doi.org/10.1061/JENMDT.EMENG-7141

Digital Object Identifier (DOI):
10.1061/JENMDT.EMENG-7141

Link:
Link to publication record in Edinburgh Research Explorer

Document Version:
Peer reviewed version

Published In:
Journal of Engineering Mechanics

Stiffness Characteristics of Composite Beams and Application in Damage Identification

Yu Gu [1], Yong Lu, F.ASCE [2*]

[1] PhD candidate, Institute for Infrastructure and Environment, School of Engineering, The University of Edinburgh, Edinburgh EH9 3JL, UK. Email: Yu.Gu@ed.ac.uk

[2*] Professor, Institute for Infrastructure and Environment, School of Engineering, The University of Edinburgh, Edinburgh EH9 3JL, UK. Corresponding author, Email: yong.lu@ed.ac.uk

Abstract

Composite structures are commonly used in civil engineering; a typical example is a bridge deck consisting of concrete slabs and steel girder beams, where shear connectors are used to connect the concrete slabs and steel beams to form a composite structure. The structural performance of a composite structure is well understood to depend not only on the properties of the primary components (slabs and steel beams) but also on the properties and condition of the shear connectors. Therefore, in a structural health monitoring and damage identification process, it is imperative to distinguish the damages in the primary components and in the shear connectors. In the existing literature concerning damage assessment of composite structures, however, there is generally a lack of differentiation between the damages in the two distinctive groups of constituent entities, and oftentimes the damages are simply treated in terms of the gross flexural stiffness with the use of an equivalent Euler-Bernoulli beam. This could result in a false identification of the actual severity of the damages and even misleading results. In this study, the basic mechanics governing the equivalent flexural rigidity and its distribution in a composite beam are investigated analytically, and the essential differences between the component beam damage and the shear connector damage on the distribution of the flexural rigidity is examined by numerical simulations. On this basis, the feasibility of differentiating the two types of damage from a damage identification process using vibration information, namely the natural frequencies and mode shapes, is demonstrated by means of a finite element model updating procedure.

Keywords: Composite beam, composite effect, damage identification, flexural rigidity, shear connector, vibration properties

Introduction

In structural health monitoring, damage identification plays an important part. In practice, the monitoring or assessment is still primarily based on dynamic properties, chiefly natural frequency and mode shape data. These dynamic properties are generally related to transverse movements, which in turn depend upon the flexural properties, namely the overall flexural stiffness and the local flexural rigidity and its distribution.

Many critical structures, such as road bridges and viaducts, often involve composite elements - a typical example would be bridge decks. As is well understood, the mechanical behaviour of a composite beam, particularly the global and local (sectional) stiffness, is affected by the properties of the "component beams", as well as the properties of the shear connectors which effectively enable the composite effect. However, in the existing damage identification literature, especially regarding vibration-based techniques, composite structures such as bridge decks are often treated as monolithic structures. Accordingly, structural parameters are identified in terms of gross composite beam flexural parameters without differentiating between the primary beam sections (referred as component beams hereinafter) and the condition of the shear connectors.

For example, in some studies, a composite beam is simplified as an Euler beam. Talebinejad et al. (2011) examined four mode shape-based approaches for identifying damage to a long-span cable-stayed composite bridge using simulated acceleration data. In their study, the composite deck is modelled by 58 beam elements with the equivalent properties of the composite section. To validate their FE model, the mode frequencies calculated by their finite element (FE) model are used to compare with the measured mode frequencies. It is noted that the frequency difference between the measured and calculated values gradually increased from -4.6% of the fundamental mode to 4.41% of the 7th mode. Shu et al. (2013) used the statistical property of the structural dynamic responses as damage indexes and an Artificial Neural Network (ANN) to detect damage to a railway composite bridge, and a FE model with Euler beam elements was used to represent the composite railway bridge. In their study, the reduction of the equivalent bridge section stiffness is used to simulate the damage.

In some other studies, it is realised that simplifications that often exist in the process of developing a FE model, for example geometry, boundary conditions or material properties, could lead to errors in the damage assessment results. As an improvement, two component beams connected by shear connectors were employed to simulate the composite beam structure.

However, the specific influence of shear-connector parameters on the flexural dynamic response of the overall structure was not considered in the assessment procedure. For instance, Malveiro et al. (2018) presented a model updating procedure aided by a genetic algorithm (GA) to obtain the FE model parameters for a composite steel-concrete railway viaduct. These parameters included the geometry and material properties of the concrete slab, steel girder, ballast layer, and stiffness properties of rail pads and supports. However, the properties of the shear connectors between the concrete slab and steel girders were not included. Tan et al. (2020) used vibration characteristics and an ANN to develop and apply a procedure focusing on detecting damage in a composite slab-on-girder bridge structure consisting of a reinforced concrete slab and three steel beams. The shear connectors in the 3-D FE model were set as rigid connections in the updating process, which means the stiffness of the shear connectors is assumed to be infinitely large, and therefore any variation in the composite and overall structural effects due to possible damage to the shear connectors was not taken into account.

Many instances have shown that when a shear connector cannot withstand the shear force or the sliding displacement exerted on it, the shear connector may fail before the other components reach their respective failure state (Queiroz et al., 2007). Besides, a shear connector may not be as effective as assumed in the design due to aging of the shear connector or the material surrounding it. Hence, treating a composite beam as an Euler beam or not considering the effect of damage in the shear connector properly in a damage assessment process could lead to incorrect identification of the actual conditions and potentially misleading results in case serious damage to shear connectors occurs.

As a matter of fact, the correlation between the flexural stiffness of a composite beam and shear connector damage is far more complicated than that with typical cross-sectional damage such as a crack. This is because the gross flexural stiffness can be affected by a) variation in the composite conditions, i.e. the properties in the shear connectors or bonded interface, and b) changes in the component beam properties, namely the nominal Young's moduli, or more generally the flexural rigidities of the component beam sections. As will be shown later in this paper, the effect of damage in the shear connectors on the stiffness and local rigidity of a composite beam will exhibit very different characteristics comparing to that caused by direct damage to the component beams.

In the composite beam literature, theoretical solutions have been developed for the evaluation of the gross flexural stiffness of the component beams considering the effects of the shear connector stiffness, as well as the rigidity of the component beams, under an intact situation. Based on the classical beam model coupled with interlayer slip, Girhammar and Gopu (1993) presented the governing differential equations in terms of the lateral deflection of a partial-interaction composite beam, and derived general closed-form solutions for displacement functions under static loads. The term 'partial interaction' here refers to the situation where the stiffness of the shear connection is finite, and as a result, shear slip exists between two component beams (Oehlers et al., 1997). In contrast, 'full interaction' refers to the situation where no shear slip exists between two component beams, which also means a full composite effect. These two terms will be adopted in the above context in the present paper. For concrete-steel composite beams, Zona et al. (2005) also pointed out the interlayer slip between the steel and concrete components must be taken into consideration in structural models of composite structures for accurate analytical response predictions. Girhammar and Pan (1993) further investigated the dynamic behaviour of an intact composite beam with partial interaction and derived general closed-form solutions for the displacement functions and internal action under dynamic loads. Correspondingly, an approximate solution for the eigen frequencies was proposed.

Nie and Cai (2003) put forward the governing differential equation with respect to the shear slip between two component beams, and subsequently derived the expression of shear slip and shear slip strain distribution along the composite beam under a midpoint load scenario as an example. In addition, considering three different static loading types and using the added curvatures derived from shear slip strain, they provided formulas for the calculation of the maximum deflection of a composite beam. Xu and Wu (2007) further investigated the static and dynamic behaviour of partial-interaction composite beams by considering the effect of transverse shear deformation and rotary inertia (i.e. using Timoshenko's beam theory). Correspondingly, the mode frequencies of the composite beam under free vibration were established.

Apart from the above theoretical studies on the basic mechanics of composite beams, some research has been conducted concerning the condition and damage assessment of composite beams, using typically FE model updating or ANN based assessment schemes. For example, Xia et al. (2007) conducted a FE model updating procedure of the whole structure of an actual bridge. In their study, more than one hundred updating parameters, including boundary conditions, bearings, girders, slab, as well as shear connectors, were included in a standard model updating procedure based on the measured frequencies and mode shapes from a field test, which included 133 measurement points and 11 modes. The results showed that the conditions of the girders, shear connectors and bearings were in a good state, but the entire slab had some degree of deterioration. Although these results were supported by visual observation, there was no proof or demonstration that the results coming out of the standard FE model updating procedure for both sets of shear connectors and component beam parameters, especially the shear connector parameters, were of good accuracy or physically meaningful.

Sadeghi et al. (2021) conducted a study on damage identification in concrete-steel composite beams and proposed the use of modal strain energy via a regression ANN to identify damages in concrete, steel and the interface layer. However, like some other studies referenced in the paper (e.g. Xia et al. 2007) in which interface damage was also included in an identification process, they did not discuss the underlying relationship between the vibration measurements (be it mode shapes, frequencies, or modal strain energy) and the flexural rigidity, or how the flexural rigidity and its distribution are affected differently by the two groups of the parameters.

In summary, despite the various developments in the theoretical mechanics study and some applications in the damage assessment of composite beams, there is a lack of systematic information and guidance with regard to a) the characteristics of the flexural rigidity of a composite beam and its distribution over the beam length, b) the specific effect of the local shear connector condition as compared to that of the changes in the component beam stiffness on the local and global flexural stiffness of a composite beam, and c) how the above effects should be effectively incorporated into a structural health monitoring and damage identification process.

This paper presents a systematic investigation into the effect of the stiffness of individual shear connectors, as compared to that of the component beams, on the flexural rigidity and its distribution in a composite beam, and subsequently on the dynamic properties in terms of mode shapes and natural frequencies. This paves the way for separating the two groups of parameters, i.e. the rigidity of the component beams and the stiffness of the shear connectors, in a subsequent identification process using commonly measured transverse vibration data. A theoretical study is firstly carried out to evaluate the inter-relationship between the stiffness of the constituent parts, i.e. the shear connectors and the component beams, and the gross transverse flexural stiffness of the composite beam in an undamaged condition. It will be demonstrated that unlike an Euler beam with an integral cross-section, where the flexural rigidity is a constant, the (equivalent) flexural rigidity of a composite beam is affected not only by the constituent properties of the beam but also by the load patterns. Furthermore, the flexural rigidity of the composite beam decreases with the decrease of the "effective length" (or increase of the order of vibration modes), and this trend tends to become more gradual and eventually approaches the non-composite flexural rigidity.

An FE model is then involved to investigate further the unique mechanical features of composite beams by looking into the interface shear slips, shear slip strains and the distributed flexural rigidity in detail. With the FE model, damages in the component beams and in the shear connectors are subsequently introduced to investigate the distinctive effects of these two types of damage on the overall structural stiffness and the distributed flexural rigidity, and thereby the dynamic properties, in a composite beam. Finally, a genetic-algorithm (GA) aided FE model updating procedure is used to actually identify the two separate types of damages in a composite beam.

Theoretical Analysis of Stiffness Characteristics of Composite Beams under Static Loading

Theoretical analysis of composite beams has been conducted extensively in the literature, with the interest being primarily focused on the global beam response such as overall stiffness and deflection rather than the distribution of the flexural rigidity (Girhammar and Gopu, 1993, Wu et al., 2002, Nie and Cai, 2003). However, for damage identification based on transverse vibration data, a thorough understanding of the characteristics of the distributed flexural rigidity in a composite beam is necessary. With this in mind, in this section the equivalent sectional rigidity distributions of a composite beam under different loads are explicitly established on the basis of the existing composite beam theory. For simplicity in the derivation, a simply supported beam is considered. It is worth noting that, while the detailed solutions are dependent upon the chosen boundary conditions, the main characteristics of interest, including the effects of the external load patterns and the effective length on the flexural rigidity of the composite section, are generally applicable. It will be demonstrated that the flexural rigidity distribution in a composite beam is not only dependent internally upon the properties of the component beams and the shear connectors, but also externally on the types of loads. Subsequently, a static load analogy is employed to investigate the sectional rigidity and its distribution in a composite beam under free vibration.

Basic theory of deformation and stiffness of a composite beam

A typical composite beam consisting of two component beams connected by shear connectors is shown in Fig. 1. The beam is assumed to be on simple supports, which may also be regarded as representing a beam segment between two contra-flexure points in a more general beam setting. Let the span length be L, and the depths of the concrete and steel beam components be h_c and h_s, respectively. The origin of the x-y system is placed at the mid-span. $q(x)$ denotes the external transverse load as a function of x along the beam.

An elastic analysis of a composite beam is generally based on the following assumptions (see e.g. Girhammar and Gopu, 1993): (1) All of the constitutive materials behave elastically, and the deformations are small. (2) The shear connectors between the two component beams are uniformly spaced along the length of the beam. (3) No transverse separation at the contact interface, which means both component beams have the same curvature at any cross-section. (4) For simplicity, the section is symmetric about its vertical axis. (5) The interface friction is not taken into account.

Typical composite beams used in practical applications fall into a partial composite design, and consequently upon loading a shear slip occurs at the interface of the two component beams, leading to an additional deflection when compared to the corresponding full interaction composite beam. There may be different routes to solving the additional (and hence the total) deflection. In order to relate specifically to the condition of the shear connectors, herein the solution towards the flexural rigidity is sought through combining an exact relationship between the additional curvature and the interface slip according to Wu et al. (2002) and a solution procedure for the interface slip proposed by Nie and Cai (2003).

In general, the equivalent flexural rigidity of a composite section at location x may be expressed as

$$EI(x) = \frac{M(x)}{\phi(x)} \tag{1}$$

in which $\phi(x)$ is the curvature of the composite beam at x under bending moment M(x).

The curvature $\phi(x)$ may be treated as a combination of the curvature as if the cross-section is fully integrated, i.e. without the interface slip, $\phi_{full}(x)$, and an "additional curvature" which is induced due to the interface slip, $\Delta\phi(x)$:

$$\phi(x) = \phi_{full}(x) + \Delta\phi(x) \tag{2}$$

and

$$\phi_{full}(x) = \frac{M(x)}{EI_{full}} \tag{2a}$$

where EI_{full} is the flexural rigidity of the composite beam with a perfect bond between the two component beams, i.e. the full-interaction rigidity.

The additional curvature $\Delta\phi(x)$ due to interface slip can be established, referring to Fig. 1(b), by considering the cross-sectional equilibrium and compatibility conditions (Wu et al., 2002), leading to:

$$\Delta\phi(x) = \frac{(E_sA_s)(E_cA_c)}{EI_{full}(E_cA_c+E_sA_s)} d_{cs}\varepsilon_s(x) \tag{3}$$

where ε_s is the relative slip strain at interface, d_{cs} is the distance between the two centroids of the upper (concrete) and lower (steel) beam cross-sections, E_s is elastic modulus of the lower beam; E_c is elastic modulus of the upper beam, and A_c and A_s are the area of the upper and lower beam cross section, respectively. $\varepsilon_s(x) = \frac{dS(x)}{dx}$, where S is the shear slip.

The shear slip $S(x)$ at the interface between the top (concrete) and bottom (steel) beams can be expressed as:

$$S(x) = \int_0^x \varepsilon_{cb}dx - \int_0^x \varepsilon_{st}dx \tag{4}$$

where ε_{cb} is the strain at the bottom of the upper beam; ε_{st} is the strain at the top of the lower beam.

Differentiating Eq. (4) and considering internal action relationship gives the relative slip strain (ε_s) at the interface (Nie and Cai, 2003):

$$\varepsilon_s(x) = \frac{dS(x)}{dx} = \varepsilon_{cb}(x) - \varepsilon_{st}(x) = \phi(x)d_c - \frac{C(x)}{E_cA_C} - \frac{T(x)}{E_sA_s} \tag{5}$$

where ϕ *is* curvature of the composite beam, C is compression in the upper (concrete) section and T is tension in the lower (steel) section, which are directly related to the bond or shear stress at the interface of the two component beams, thereby the shear connector stiffness and the shear slip.

Differentiating Eq. (5), and considering the force and moment equilibriums and curvature compatibility (Nie and Cai, 2003), the governing differential equation in terms of the shear slip S under a general loading condition can be given as:

$$\frac{d^2S(x)}{dx^2} = \delta^2 S(x) - \delta^2 \zeta V(x) \tag{6}$$

where $\delta^2 = K_s/(A_1 E_s I_0 p)$, $\zeta = A_1 d_{cs} p/K_s$, in which K_s is the shear stiffness of the individual shear connector, p is the longitudinal pitch (spacing) of shear connectors, $A_1 = A_0/(I_0 + A_0 d_{cs}^2)$ in which $A_0 = (A_s A_c)/(n_E A_s + A_c)$, $I_0 = \frac{I_c}{n_E} + I_s$ and $n_E = E_s/E_c$. I_s, I_c are the moment inertia of the steel and concrete beam cross section, respectively. $V(x)$ is the internal shear force acting on the whole composite beam cross-section at point *x*.

Solving Eq. (6) for *S(x),* and then using Eqs. (5) and (3), the additional curvature distribution corresponding to different types of loads can be obtained, which can then be utilised to calculate the flexural rigidity distributions according to Eqs. (2) and (1).

Composite Beam Flexural Rigidity Distributions under Different Types of Loads

a) Theoretical formulation

Three typical loading conditions, namely a mid-span point load *P*, a uniformly distributed load q, and a pure bending with a constant bending moment M_0, are analysed in this section to examine the flexural rigidity distributions.

For the boundary conditions concerning slip, at $x = 0$, slip $S = 0$ under these three loads. At the beam end, i.e., $x = L/2$, the compression C in the upper beam section and tension T in the lower beam section are both zero, thus, referring to Eq. (5), the slip strain becomes:

$$\frac{dS(x)}{dx} = \phi(x) d_{cs} \tag{7}$$

Under the mid-span point load and uniformly distributed load conditions, curvature $\phi = 0$ at $x = L/2$, Eq. (7) gives slip strain $\frac{dS}{dx} = 0$. Under pure bending, at $x = L/2$, $\phi \neq 0$, so considering Eq. (5), and letting $\gamma = \frac{(E_s A_s E_c A_c)}{EI_{full}(E_c A_c + E_s A_s)} d_{cs}$, Eq. (7) can be further represented by:

$$\frac{dS(x)}{dx} = [\phi_{full}(x) + \Delta\phi(x)] d_{cs} = \left(\frac{M_0}{EI_{full}} + \frac{dS(x)}{dx} \cdot \gamma\right) d_{cs} \tag{8}$$

Rearranging Eq. (8) gives:

$$\frac{dS(x)}{dx} = \left(\frac{M_0}{EI_{full}}\right) \cdot \frac{d_{cs}}{(1-\gamma d_{cs})} \tag{9}$$

By the above boundary conditions, the shear slip S can be solved from Eq. (6). The added curvature distribution can be determined through Eqs. (5) and (3). Subsequently, the distribution of the total curvature can be obtained. Given the bending moment at x is $M(x)$, the nominal flexural rigidity at different positions of the composite beam can be further written from Eq. (1) as:

$$EI(x) = \frac{M(x)}{\phi_{full}(x)+\Delta\phi(x)} = \frac{M(x)/\phi_{full}(x)}{1+\Delta\phi(x)/\phi_{full}(x)} = \left(\frac{1}{1+\Delta\phi(x)/\phi_{full}(x)}\right) EI_{full} \tag{10}$$

Obviously, the larger the slip strain at a particular position, the larger the added curvature, and subsequently, the smaller the flexural rigidity at the position.

Omitting the solution details, the distributed flexural rigidity of the composite beam under the three loading conditions are determined as follows.

For mid-span point load:

$$EI_{mpl}(x) = \frac{1}{1+EI_{full} \cdot \frac{\gamma\delta\zeta(e^{-\delta x}-e^{\delta x-\delta L})}{(1+e^{-\delta L})(L/2-x)}} \cdot EI_{full} \tag{11}$$

For uniformly distributed load:

$$EI_{udl}(x) = (1/\left[1 + 8\zeta\gamma e^{-\delta x} EI_{full} \frac{e^{\frac{\delta L}{2}}(1-e^{2\delta x})+\delta x e^{\delta x}(e^{\delta L}+1)}{(e^{\delta L}+1)(4x^2-L^2)} - 8\zeta\gamma e^{\delta x} EI_{full} \frac{(e^{\delta x}+\delta x e^{\delta x})(e^{\delta L}+1)-2e^{\left(\frac{\delta L}{2}+2\delta x\right)}}{(e^{\delta L}+1)(4x^2-L^2)}\right]) EI_{full} \tag{12}$$

For pure bending (i.e. with a constant bending moment):

$$EI_{pb}(x) = \frac{1}{1+\frac{d_{cs}}{(1/\gamma-d_{cs})} \cdot \frac{e^{\left(\frac{\delta L}{2}+\delta x\right)}+e^{\left(\frac{\delta L}{2}-\delta x\right)}}{e^{\delta L}+1}} \cdot EI_{full} \tag{13}$$

b) Example composite beam

It is well known that a classical Euler beam with a fully integrated cross-section will have a uniform flexural rigidity distribution throughout the beam (except in the end regions), and it does not depend on load conditions. From the above theoretical derivations, it can be understood that the distributed equivalent flexural rigidity of a composite beam depends not only on the cross-section geometry, material properties and the shear connector stiffness, but also on the types of loads.

A conceptual "T" shaped composite beam is used here to demonstrate the distributions of flexural rigidity of the composite beam under different types of static loads. The composite beam consists of a concrete beam component at the top and a steel beam component at the bottom. The length (L) of the beam is 4 m. The widths of the concrete and steel component beams are 0.3 m and 0.05 m, respectively, and the depths of the concrete and steel component beams are 0.05 m and 0.15 m, respectively. The Young's modulus of concrete is assumed to be 26 GPa, and density is 2300 kg/m^3. The Young's modulus of steel is 205 GPa, and density is 7900 kg/m^3.

For the shear connectors, a spring is used to represent the shear resistance along the interface between the component beams provided by the mechanical action of a shear connector. The stiffness of the shear spring can be approximated by an empirical equation (Oehlers and Coughlan, 1986) as:

$$K_s = \frac{P_{st}}{d_{sh}(0.16 - 0.0017 f_c)} \quad (14)$$

where d_{sh} is the diameter of the shank of the shear connector (mm), and P_{st} is the static strength of the shear connector (MPa), which may be determined by (Oehlers and Coughlan, 1986):

$$P_{st} = 4.3 A_{sh} f_u^{0.65} f_c^{0.35} \left(\frac{E_c}{E_s}\right)^{0.40} \quad (15)$$

where f_u is the ultimate tensile strength of the shear connector material, f_c is the compressive strength of concrete

From Eq. (14) and (15), it can be seen that the stiffness of the connector not only depends on the material and geometry of the shear connector (stud) itself but also the moduli and strength of concrete. Herein we use the shear connector from a previous study (Xia et al., 2008) as an example. Each connector is made of a steel bar of 12.7 mm in diameter. The static strength of each shear connector is calculated as P_{st}= 43.4 kN and shear stiffness as K_s= 53.7 kN/mm. Furthermore, the minimum amount of the shear connectors, which is based on strength requirements (Oehlers et al., 1997), needs to satisfy the following condition:

$$N_{st} \times P_{st} \geq 0.85 \cdot f_c \cdot A_c \quad (16)$$

where N_{st} is the minimum number of shear connectors for the shear span. Considering the concrete (grade C40) axial compressive strength f_c= 26.9 N/mm^2, the cross-section area of concrete A_c = 15000 mm^2, N_{st} would be 3. In the present case, 20 shear connectors are arranged along the composite beam for a well distributed interaction between the two component beams.

Fig. 2 shows the distributions of the flexural rigidity of the composite beam under different load patterns. It can be clearly observed that the flexural rigidity distributions of the composite beam under different load patterns are significantly different. For example, under the pure bending load, the maximum and minimum flexural rigidity are 5.3×10^6 Nm^2 and 3.1×10^6 Nm^2, respectively, with a variation of about 40%, whereas for a uniformly distributed load, the maximum and minimum flexural rigidity are 4.8×10^6 Nm^2 and 4.4×10^6 Nm^2. For a mid-span point load, the flexural rigidity is minimum of 4.3×10^6 Nm^2 at the mid-span, and maximum 5.3×10^6 Nm^2 at the end, respectively.

From the above results, it can also be understood that, without an explicit consideration of the shear connectors it would not be possible to conduct an appropriate assessment of the structural condition of a composite beam based on vibration information. The available vibration information may lead to the identification of a nominal flexural rigidity profile, but how this can then be related to the structural state in the composite beam would require the knowledge about the contributions of both the component beams and the shear connectors. Simplifying a composite beam as an Euler beam could result in inadequate and even misleading assessment of the actual structural condition.

Derivation of the Flexural Rigidity Distribution of a Composite Beam for Free Vibration Modes Using a Static Load Analogy

For a beam in free vibration, according to the D'Alembert's principle, the inertia force can be looked upon as an external load applied to the beam in a static condition. From the analytical solution of the mode shape for the first mode, it can be understood that the distribution of the acceleration, and hence the inertial force, follows a sinusoidal wave function. Such a load diagram is presented in Fig. 3, where 'w_0' is a constant value related to the acceleration amplitude over the beam length.

The vertical reaction force at support B is calculated as:

$$R_B = \int_0^{\frac{L}{2}} w_0(\rho_c A_c + \rho_s A_s)\, cos\left(\frac{\pi}{L}x\right) dx = \frac{w_0}{\pi}(\rho_c A_c + \rho_s A_s)L \tag{17}$$

where ρ_c and ρ_s are the mass density of concrete and steel, respectively.

The internal shear force and bending moment at point x can be obtained as:

$$V(x)_{sin} = R_B - \int_x^{\frac{L}{2}} w_0(\rho_c A_c + \rho_s A_s)\, cos\left(\frac{\pi}{L}x\right) dx$$
$$= \frac{w_0(\rho_c A_c+\rho_s A_s)L}{\pi} sin\left(\frac{\pi}{L}x\right) \tag{18}$$

$$M(x)_{sin} = \frac{w_0(\rho_c A_c+\rho_s A_s)L^2}{\pi^2} cos\left(\frac{\pi}{L}x\right) \tag{19}$$

The boundary conditions concerning S can be expressed as: $S = 0$ at $x = 0$ and slip strain $\frac{dS}{dx} = 0$ at $x = L/2$.

Substituting Eq. (18) into Eq. (6) and solving with the above boundary conditions gives

$$S(x)_{sin} = \frac{\delta^2 w_0(\rho_c A_c+\rho_c A_c)\zeta L^3}{\delta^2 L^2 \pi+\pi^3} sin\left(\frac{\pi x}{L}\right) \quad for\ 0 \le x \le \frac{L}{2} \tag{20}$$

Correspondingly, the slip strain solution:

$$\varepsilon_s(x)_{sin} = \frac{dS(x)_{sin}}{dx} = \frac{\delta^2 w_0(\rho_c A_c+\rho_c A_c)\zeta L^2}{\delta^2 L^2+\pi^2} cos\left(\frac{\pi x}{L}\right) \tag{21}$$

Using Eqs. (3), (10), (19), and (21), the distribution of flexural rigidity of the composite beam under a sinusoidal distributed load can be determined as:

$$EI(x)_{sin} = \frac{1}{1+EI_{full}\cdot\frac{\pi^2\delta^2\zeta\gamma}{\delta^2 L^2+\pi^2}} EI_{full} \tag{22}$$

Fig. 4 presents the distributed flexural rigidity of the composite beam under a sinusoidal distributed loading for different beam lengths while all other properties are the same. The length values are L, L/2, L/3 and L/4, which may be regarded as representing the distance between two adjacent nodal points along the composite beam in the first 4 mode shapes, respectively.

Firstly, it can be observed that $EI(x)_{sin}$ is a constant value in each length case, i.e. it has a uniformly distributed rigidity along the composite beam. Since the static sinusoidal distributed load is analogous to the distribution of the inertial force in the vibration under a particular mode, it can be understood that a similar distribution of the (equivalent) flexural rigidity will occur under the corresponding mode.

Secondly, it can also be observed that $EI(x)_{sin}$ gradually decreases with the decrease in the beam span length and eventually approaches the non-composite cross-section rigidity, denoted as EI_{sum}, which is the sum of the cross-section rigidity of the component steel beam and concrete beam on their own.

This phenomenon indicates the trend of change in the equivalent sectional rigidity for different vibration modes and will be further discussed in association with the natural frequencies of the composite beam in the next section.

Stiffness Characteristics and Equivalent "Modal" Sectional Rigidity of Composite Beams from Direct Dynamic Formulation

In this section, the interrelationship between the equivalent flexural rigidity of a composite beam and the order of the vibration mode, herein referred to as the "modal flexural rigidity", is further examined in accordance with the direct dynamic formulation for a composite beam, and a concept of "effective length" is proposed for the quantification of the equivalent modal sectional rigidity under different modes.

The nth mode frequency of a composite beam ω_{cp-n} may be obtained by (Wu et al., 2007):

$$\omega_{cp-n}^2 = \left(1 - \frac{\beta^2 - 1}{\beta^2 + \alpha^2/\xi^2}\right) \omega_{full-n}^2 \tag{23}$$

where $\alpha^2 = k_s\left(\frac{1}{E_c A_c} + \frac{1}{E_s A_s} + \frac{{d_{cs}}^2}{EI_{sum}}\right)$, k_s is the distributed shear stiffness of the shear connector; $k_s = K_s/p$, $\beta^2 = \frac{EI_{full}}{EI_{sum}}$, $\xi = n\pi/L$. ω_{full-n} is the nth mode frequency of the corresponding full-interaction composite beam, and

$$\omega_{full-n} = \xi^2 \cdot \sqrt{\frac{EI_{full}}{\rho A_{full}}} \tag{24}$$

where $\rho A_{full} = \rho_c A_c + \rho_s A_s$.

The nth natural frequency of a composite beam may also be written in terms of the equivalent flexural rigidity of the composite beam at nth mode (EI_{cp-n}) in a format similar to the full-interaction composite beam in Eq. (24) as:

$$\omega_{cp-n} = \xi^2 \cdot \sqrt{\frac{EI_{cp-n}}{\rho A_{full}}} \tag{25}$$

Considering Eqs. (23) and (25), the equivalent flexural rigidity of the composite beam at nth mode EI_{cp-n} can be written as:

$$EI_{cp-n} = \left(1 - \frac{\beta^2 - 1}{\beta^2 + \alpha^2/\xi^2}\right) EI_{full} \tag{26}$$

From Eq. (26), it can be understood that an increase of the mode order *n* leads to a decrease in the equivalent flexural rigidity EI_{cp-n}.

The same simply supported composite beam used earlier in Example Composite Beam section is recalled here to demonstrate this phenomenon. In this beam, β^2 is calculated as 2.05, α^2 is calculated as1.77 and the distributed shear rigidity of the shear connector k_s is calculated as 268.5 kN/mm^2.

Fig. 5 shows the variation of $EI_{cp-n}/\ EI_{full}$ with the mode number *n*. It can be observed that with an increase in the mode order, EI_{cp-n} decreases from about 78% of the corresponding EI_{full} for the first mode to about 55% under the third mode, and then more gradually decreases to approach the non-composite EI_{sum}, which is 48% of EI_{full} in this particular beam.

By comparing Eqs. (22) and (26), it can be found that the nominal rigidity determined from the direct dynamic formulation EI_{cp-n}, with *n* being the corresponding mode order are the same as the nominal rigidity of a composite beam derived from using the static load analogy under a sinusoidal load distribution, EI_{sin-n}, with a beam length of *L*/*n*. Since *L*/*n* is actually the distance between two adjacent contra-flexure points of the n-th mode shape, the fact that EI_{cp-n}coincides with EI_{sin-n} indicates that the equivalent stiffness of a composite beam under a particular mode (*n*) is dictated by *L*/*n*, i.e. the “effective length”.

With the increase of the mode order, the effective length within which the composite effect develops also decreases, resulting in a decrease of the equivalent flexural stiffness and eventually approaching EI_{sum}, in which no composite effect exists. This phenomenon suggests that higher modes beyond a certain order would not be sensitive to the condition of the shear connectors in a composite beam.

In summary, the composite effect decreases with the increase of the mode order, even under an intact situation. This is distinctively different from an Euler beam (representing a solid or fully integrated beam), which possesses a constant flexural rigidity irrespective of different modes. In the context of vibration-based damage identification, the following arguments may be made:

1) An assessment of the condition of a composite beam from transverse vibration properties must take care of the varying equivalent rigidity with varying modes – this is fundamentally different from the classical Euler beams where the flexural rigidity at any given section is a constant (assuming a uniform cross section along the beam length) and is independent of the mode order; and

2) Consequently, when damage to the composite effect occurs, the correlation between the damage in the shear connectors (or bond interface) and the vibration properties will become complicated, and without effective resolution of such complexity, the traditional rigidity-based inverse procedure will not be physically correct.

The following sections will present further insight into the variation and complex effect of shear connector damage on different modes and the modal properties.

Numerical Study on General Effects of Component-Beam and Shear-Connector Damages on Stiffness Distribution and Modal Properties

In this section, an FE model for a composite beam is developed and validated for the purpose to investigate the general effects of damage in the component beams and damage in shear connectors on the flexural properties of the composite beams.

Finite Element Model Set-Up

Fig. 6 shows a 2D FE model of a simply supported composite beam consisting of two rectangular component beams. The two component beams have an equal depth of 0.05m and a width of 0.3m, and the length of the beam is 2m, giving a length-to-depth ratio of 20. The beam is modelled with CPS4R elements, and it is meshed into 40 layers over the depth and 800 layers along the beam length.

For the basic case, the Young's modulus of the top and bottom beams are both set as 26 GPa. The density of each component beam is set as 2300kg/m^3. The corresponding theoretical cross-section rigidities for the top beam and bottom beam are the same and equal to 8.125×10^4 Nm^2. Thus, the *EI* ratio between them is 1:1, and EI_{full} / EI_{sum} = 4.

Totally 20 discrete shear connectors are arranged uniformly along the beam length, and they are designated as No. 1 to No. 20 consecutively from left to right. A function named 'connector' in ABAQUS is used to simulate the function of the shear connector in the FE model. Based on the assumption that no transverse separation occurs at the contact interface (and therefore, the curvature is the same for both component beams at any cross-section), the axial stiffness of the shear connectors is assumed as infinitely large; in other words, the concrete slab and steel girder is coupled along the depth direction. The lateral stiffness (along the beam length direction) of each shear connector is assumed to be 40 kN/mm. From Eq. (26), the equivalent flexural rigidity of this composite beam under the intact situation is calculated to be 59% of the EI_{full}, which is 3.776×10^5 Nm^2.

Finite Element Model Validation

The static and dynamic properties of the composite beam calculated by the theoretical method is used to validate the FE model. Table 1 shows a comparison of the mode frequencies obtained from the FE model with the theoretical values (Eq. (23)). It can be observed that the comparison is generally good, with the theoretical mode frequencies being slightly higher than the FE results. With an increase in mode order, the discrepancy increases from 0.34% for the first mode to 4.68% for the fifth mode. This may be attributed to the fact that in the FE model, the shear connectors are discretely distributed, whereas in the theoretical model, the effect of shear connectors is "equivalently" treated as a continuous distribution. Moreover, the theoretical model is based on a 1D beam formulation without considering the 2D effects at the end regions.

Besides the above validation with the modal information, two static loads, designated as "Load 1" and "Load 2", are applied to the FE composite beam model to simulate the inertia force in the 1st and 2nd-mode free vibration, as shown in Fig. 7. The corresponding flexural rigidity distributions are compared to the theoretical values.

The deformation shapes of the composite beam under Load 1 and Load 2 are shown in Fig. 8. The deformation shapes are similar to the corresponding mode shapes.

The shear slip and slip strain calculated by the FE model and theoretical formulas under the Load 1 and Load 2 scenarios are compared and presented below. The numerical shear slip and slip strain curves are extracted from 101 pairs of sample points located at the bottom of the upper beam and top of the lower beam in the FE model. It is worth noting that to eliminate the effect of the concentration of stress brought about by the discrete shear connectors, the curves of the slip strain are smoothed by averaging the two adjacent data points.

Fig. 9 presents the shear slip and shear slip strain under the Load 1 scenario. It can be observed that the shear slip distribution calculated by the FE model matches the theoretical shear slip distribution, which is a sinusoidal curve. The shear slip at the mid-point of the beam is zero and gradually increases to the maximum value at the two ends of the beam. As the shear force incurred in a single shear connector is proportional to the shear slip between steel and concrete beams at the corresponding location, the shear connectors in the end regions will incur higher shear force between the top and bottom beams than the shear connectors in the middle region. This means that the shear connectors in the side regions are more critical in forming the composite effect than the shear connectors near the middle section, and consequently can be anticipated to exhibit higher sensitivity to the first mode related information. For the shear slip strain, it can be observed that the shear slip strain calculated by the FE model also coincides the theoretical shear slip strain and follows a sinusoidal curve.

The shear slip and shear slip strain of the composite beam under the Load 2 scenario is presented in Fig. 10. Similar to the Load 1 scenario, the shear slip and shear slip strain are sinusoidal curves but in a whole cycle. As the shear connectors are engaged more or less depending upon the magnitude of the shear slip, under the Load 2 scenario the shear connectors near the beam end and middle regions (No.1, 10, 11 and 20) contribute more to the composite effect while those near the first and third quarter points of the beam (No.4, 5, and 14, 15) contribute less.

To evaluate the curvature from the FE results, the vertical displacements along the bottom surface of the FE model for the composite beam are extracted at refined sample points, and the curvature $\phi(x)$ is calculated by finding numerically the second derivative of the displacement shape. The distributed flexural rigidity is then calculated by dividing the bending moment by the curvature at the corresponding location.

Fig. 11 compares the $EI(x)_{FE}$ under the two load scenarios with the $EI(x)_{sin}$ calculated for the whole and one-half of the beam length (i.e. the effective lengths of mode 1 and mode 2) respectively. The corresponding $EI_{full}(x)$ values calculated by the FE model and theoretical method are also presented on the graph for reference. It should be noted here that, as the curvature calculated by the 2D FE model is complicated in the end regions, the values of the $EI(x)_{FE}$ within a length equal to the depth of the beam from the boundaries are not presented in the graphs.

It can be observed that the *EI* distributions of the FE model agree well with the theoretical results. The results further confirm that the composite beam in the n^{th} mode is equivalent to dividing the beam into *n* composite beams with an effective length of *L*/*n*. This indicates that studying the damaging effect from a single effective length can be representative, and this will be presented in the next section.

General Effects of Damage in the Component Beams and Damage in the Shear Connectors on the Composite Beam Properties

It is understood that the transverse vibration properties (frequencies and mode shapes) of a beam are affected directly by the flexural stiffness. Therefore, it is important to look at how changes in the shear connectors and in the component beams affect the local and overall flexural stiffness. In this section, the component beam and shear connector damages are introduced into the composite beam, and the corresponding effects on the distributed flexural rigidity and dynamic properties are presented and discussed. The way of calculating the distributed flexural rigidity from the FE results is the same as described in the previous section (FE Model Validation). As a representation, the composite beam under Load 1 is employed. The relative effect from this scenario can be extended to higher vibration modes, for example mode 2 (Load case 2) is actually similar to Load case 1 but with a halved effective length.

For the component beam damage scenarios, the upper beam (mimicking a concrete beam or slab) is divided into 10 segments along the length direction. The damage to the component beam is then simulated by reducing the stiffness (Young's modulus) in individual segments. Four damage scenarios are firstly created, and in each scenario, one of the five upper beam segments within the left half span, except segment No.1, is made to have a 50% reduction of the initial stiffness. It should be noted this 50% reduction of stiffness is applied only "locally" in one of the 10 segments along the length of the beam, and this is considered to be realistic in the sense that, for example, a cracked reinforced concrete beam section could introduce an order of 50% reduction in the local flexural rigidity.

For the shear connector damage, there are 20 distributed shear connectors, so dividing them individually would mean a resolution of a 1-20th grid along the beam length. To be in line with the component beam damage resolution explained above, i.e. over about 1-10th of the span length, and considering that the sensitivity of damage in the shear connectors is generally lower than the bending damage in the component beams, two adjacent shear connectors are grouped into one set of the same parameter for the damage identification. Accordingly four damage scenarios are designed. In the first damage scenario, the shear connectors No.1 and No.2 are removed (refer to Fig. 6). In the second and third damage scenarios, two adjacent shear connectors of No.5 to No.8 are successively removed, respectively. In the fourth damage scenario, the shear connectors of No.10 and 11 are removed.

Fig. 12 and Fig. 13 show the distributions of the flexural rigidity of the composite beam normalised with respect to the intact flexural rigidity (EI_{intact}) under the four component beam damage scenarios and the four shear connector damage scenarios, respectively.

Referring to Fig. 9, it can be observed that the greater the slip at the position of a shear connector, the more significant the impact of the shear connector damage on the distributed flexural rigidity. That explains why damage of shear connectors No.10 and 11 influences only marginally the flexural rigidity distribution. In contrast, the damage in the concrete beam has a pronounced local effect on the distributed flexural rigidity along the composite beam.

From the above demonstration, it becomes clear that the distribution of the flexural rigidity reduction caused by damage in the shear connectors is distinctively different from that caused by damage in the component beams.

To further demonstrate such differences, the effect of damage in the component beam and in the shear connectors is examined in terms of the modal information. For this purpose, two component beam damage scenarios and two shear connector damage scenarios are used to examine the variation in the modal information variation caused by these two types of damage. The two shear connecter damage scenarios consist of 1) the removal of the shear connectors No.5 and No.6, and 2) the removal of shear connectors No.10 and 11. The two component beam damage scenarios consist of the reduction of the beam stiffness in segments No.2 and 5 by 50%, respectively.

Fig. 14 (a) shows a comparison of the first-mode shape curvatures between the two shear connector damage scenarios. For the scenario with the removal of the shear connectors No. 5 and 6 , the mode shape curvature is markedly altered throughout the entire left half of the beam, i.e., the effect propagates well beyond the location of the two damaged shear connectors. It is interesting to note that the removal of shear connectors No.10 and 11 affects little the mode shape curvature. This phenomenon echoes very well the findings shown in Fig. 9, in that the shear slip around the mid-span of the composite beam is minimal for the first mode shape, thus the shear connectors in the mid-span region make little contribution in the composite effect for the first mode. In contrast, the damage to the component beam directly affects the modal curvature at the immediate position of the damage, as shown in Fig. 14 (b).

Table 2 summarises the first six mode frequencies of the four damage cases in comparison with the frequencies of the intact composite beam. A significant effect can be observed on the first mode for the scenario of removing shear connectors No.5 and 6, whereas the influence of this damage on the second mode is minimal, due to the particular slip distribution under this mode as explained previously. Shear connectors No.10 and 11, on the other hand, are located in the mid-span of the beam, which are at or near the displacement peak of modes 1, 3 and 5 but at or near a contra-flexure point of modes 2, 4 and 6. Consequently, removing these shear connectors has a more pronounced effect on the natural frequencies for modes 2, 4 and 6 as compared to modes 1, 3 and 5.

Besides the damage position that can influence the percentage difference between the modal frequencies of intact and damaged composite beam, the overall composite effect corresponding to a particular mode is another factor. Generally speaking, with the increase of the mode order, the composite effect tends to diminish due to a reduced effective length; consequently, the effect of damages in the shear connectors on the modal frequencies tends also to decrease. For example, for the scenario with the removal of shear connectors No.10 and 11, the percentage difference in the natural frequencies for modes 2, 4, 6, in which the relative position of the damaged shear connectors within the corresponding effective length are comparable, decreases from -3.45% for mode 2, to -1.35% for mode 4, and to -0.65% for mode 6.

The results from the above numerical simulation show that damage in the shear connectors has a complex effect on the flexural properties of the composite beam. Despite the added complexities, however, there are distinguishable patterns in the changes of the flexural rigidities, thereby the modal frequencies and mode shapes, caused by the shear connector damages from that caused by the component beam damages. This suggests that, using the modal data extracted from transverse vibration measurements, it should be possible to identify the damages in the shear connectors, thus allowing a separation of the two groups of parameters in the identification process. The following section will demonstrate the utilisation of a GA-based FE updating procedure to identify both the shear connector damage and the component beam damage in a composite beam.

Damage Identification in Composite Beams – a Demonstrative Study

This section presents a preliminary study on the identification of damages in a composite beam using GA-aided FE model updating. It will be shown that it is possible to identify the two separate groups of damage, i.e., component beam damage and shear connector damage, with the use of vibration data.

In structural damage identification based on FE model updating, the basic idea is to "update" the FE model parameters so that the "responses" produced by the FE model, herein the dynamic properties including natural frequencies and mode shapes, match the target or measured responses from the actual structure. The updated FE parameters are then considered as representing the current state of the structure. The "match" is usually achieved by minimising an objective function or residuals formulated by the differences between the FE predicted and the target "response parameters".

Herein the FE model introduced in section Finite Element Model Setup is used to demonstrate the damage identification process. In order to extract the mode shape data, 19 measuring points are evenly arranged along the length of the beam, at an interval of L/20. As mentioned earlier, the upper beam (mimicking a concrete beam or slab) is divided into 10 segments, and the 20 shear connectors are also divided into 10 groups, each of which contains two adjacent shear connectors with the same condition. Thus, 20 stiffness parameters are put forward for updating, 10 in the component beams, and 10 in the shear connectors.

For the present illustrative purpose, a general objective function for the FE model updating is defined as the residual error consisting of the mode frequency residual value R_f and the mode shape residual value R_{ms},

$$R = R_f + R_{ms} \tag{27}$$

Many object functions have been employed for model updating in the literature (Hou and Lu, 2016, Moaveni et al., 2009). In order to minimise the influence of the basic model error, the residuals are calculated using the normalised measured and theoretical modal data with respect to their corresponding undamaged counterpart, as:

$$R_f = \frac{1}{N_f}\sum_{i=1}^{N_f} abs\left(\frac{f_{di,m}^2}{f_{0i,m}^2} - \frac{f_{di,c}^2}{f_{0i,c}^2}\right) \tag{28}$$

$$R_{ms} = \frac{1}{N_{ms}N_n}\sum_{i=1}^{N_{ms}}\sum_{j=1}^{N_n} abs\left[\left(\frac{\phi_{dm_i}^j}{\phi_{0m_i}^j}\right)^2 - \left(\frac{\phi_{dc_i}^j}{\phi_{0c_i}^j}\right)^2\right] \tag{29}$$

where f_i denotes the i-th natural frequency and ϕ_i^j denotes the j-th element in the i-th normalised mode shape vector. N_f, N_{ms} and N_n are the numbers of the natural frequencies, mode shapes and measured nodes, respectively. Subscripts 'c' and 'm' represents the FE calculated and the "measured" data, respectively, and subscripts 'd' and '0' denote the damaged and intact states of the beam, respectively.

It is worth noting that the measured data from the intact state of the structure may not be available in practice, so in such a case, the results from the FE model of the structure in the intact state may be used to approximate those measurements of the intact structure for the normalisation purpose (Xia et al., 2002).

The stiffness parameters designated for identification, namely all 10 segments in the upper beam and all 10 groups of the shear connectors, are being updated in the process, and GA is employed to facilitate the updating process in minimising the defined objective function. It is worth noting at this juncture that a FE model updating procedure based on GA has several advantages, including independency from the initial setting of the parameters being updated, and the avoidance of the calculation of the sensitivity matrix of the structure (Tu and Lu, 2008).

In the numerical simulation, firstly a particular damage state is created by assigning a specific set of "damaged" parameters for the composite beam. The modal data for the damaged structure is then computed using the FE model. These data will be used as the "measured" data with which the damage state of the composite beam will be identified through the FE model updating procedure.

With the “measured” modal data as the matching target, a sufficient number of groups of the stiffness parameters are randomly generated to represent an initial pool of possible damage states, i.e. the "population" using the terminology of GA. These groups of stiffness parameters are then introduced into the FE model group by group, and the corresponding modal data set are calculated from the FE model. Each modal data set is subsequently fed into the objective function to calculate the residual value. If the residual value meets the pre-set threshold, the corresponding damage state will be regarded as the final result. Otherwise, GA will move on to the next set of parameters to repeat the same calculation and checking process. One round of the iteration is the so-called “generation”, and “crossover” and “mutation” will occur after each generation, until a particular set of parameters is found to meet the pre-set criteria for the residual function. When this occurs, the iterative process terminates, and the distribution of the stiffness parameters will be exported, which represents the stiffness parameters of the target state of the structure.

During the preliminary trials, many combinations, including just one-type of damage were tested. It was found that both one-type damage, i.e. damage in the shear connectors only and damage in component beams only, can be successfully identified. Herein for demonstration, two damage scenarios involving a combination of a single component beam damage and a single shear connector damage are chosen as examples. The first case has the flexural rigidity of No.3 segment of the upper beam reduced to 60% of the undamaged value and the stiffness of No.3 shear connector group reduced to 10% of the undamaged value. The second case has the stiffness of No.5 segment of the top beam reduced to 60% of the undamaged value and the stiffness of No.2 shear connector group reduced to 10% of the undamaged value.

For the above two damage cases, the "measured" modal data are obtained by analysing the FE model with the two particular sets of damage parameters. In this demonstrative study, use is made of the first 5 natural frequencies and the first 3 mode shapes to calculate the residual errors, and this generally reflects the order of modes that may be reasonably measured in practice. The settings of GA are as follows: population size 100, and crossover score and mutation rate 0.8 and 0.02, respectively. The fitness limit is set to be 0.02. The interval of the stiffness parameter is set to be 1% of the undamaged stiffness for the searching process. The whole process is completed in 43 iterations and takes about 20 hours using a standard desktop PC.

Fig. 15 illustrates the results of the 20 stiffness parameters produced by the FE model updating process against the target parameters. All the stiffness parameters are updated correctly. It is worth mentioning that the first damage case involves shear connector and component beam damages which occur in the same region of the composite beam, and even in such a case, the two types of damages can be identified (therefore separated) with reasonable accuracy. These results confirm that, through an appropriate procedure (herein FE model updating), it is possible to use the modal data from the standard vibration measurements to identify damage in the two distinctive groups of parameters, i.e. shear connectors and the component beams, in a composite beam.

Conclusions

A systematic investigation has been conducted into the flexural rigidity and its distribution in a composite beam, and how these are affected by changes (damages) in the two distinctive groups of parameters, i.e. that of the shear connectors and that of the component beams. The effects of the two types of damage are then examined in terms of the dynamic properties as represented by the modal frequencies and mode shapes, thus establishing the basis for the identification of the two types of damage in composite beams using data from transverse vibration measurements. The key developments and findings of this study are summarised below.

1) Through theoretical analysis, it is established that the distribution of the equivalent flexural rigidity of a composite beam is affected by the properties of both the component beams and the shear connectors. The effect of the shear connectors is further influenced by the load patterns through the effect on the shear slip strain distribution at the interface of the component beams. This leads to different flexural rigidity distribution of the same composite beam under different types of loads, a phenomenon that differs fundamentally from a typical Euler beam.

2) The equivalent flexural rigidity of a composite beam decreases with the increase of the order of modes, even in an intact condition. This is because the effective length of the composite beam decreases with the increase of the mode order.

3) Treating a composite beam as a nominal Euler beam in a damage identification process will lead to incorrect identification and even misleading results.

4) Through FE simulation, it is found that a shear connector damage will affect the flexural rigidity and subsequently the mode shapes over a larger area (length), and this phenomenon is distinctively different from the situation with a local damage to a component beam.

5) Using a standard FE model updating procedure with the aid of GA, it is demonstrated that it is possible to identify the two distinctive types of damage, i.e. damage to a component beam and damage to the shear-connectors in a composite beam with the vibration data.

It should be noted that the above investigation and observations are aimed at demonstrating the need and the possibility of separating the component beam damage and shear connector damage in a composite beam with the vibration data in principle. However, the success of applying the FE model updating for the damage assessment in a structure relies on the sensitivity of the dynamic parameters to the damage, and this is particularly true when a single scalar residual is used as the objective function. If the dynamic parameters, as manifested in the objective function, are not sensitive enough to the structural damage parameters, it may not be feasible to identify the damage parameters successfully. In this respect, in subsequent research the involvement of a more robust regression scheme through machine learning will be explored. The damage features pertaining to the two types of damage in the composite beams, as demonstrated in this paper, need to be further examined in more realistic and practical conditions. This would require a systematic study on the sensitivities, including the size and location of damage with respect to individual modes, and with involvement of structural uncertainties and the effect of measurement errors and noise. In future work, the unique features of composite beams in terms of the two types of damage may also be exploited with a specially tailored strategy involving a staged process, in which the first stage may be focused on classifying the presence of one or both types of damage utilising their distinctive features, and the subsequent stage(s) will then quantify the respective damage severity.

Data Availability Statement

All data, models, or code that support the findings of this study are available from the corresponding author upon reasonable request.

Acknowledgements

For the purpose of open access, the authors have applied a Creative Commons Attribution (CC BY) licence to any Author Accepted Manuscript version arising from this submission.

References

Girhammar, U. A. & Gopu, V. K. 1993. Composite beam-columns with interlayer slip—exact analysis. *Journal of Structural Engineering,* 119**,** 1265-1282.

Girhammar, U. A. & Pan, D. 1993. Dynamic analysis of composite members with interlayer slip. *International Journal of Solids and Structures,* 30**,** 797-823.

Hou, C. & Lu, Y. 2016. Identification of cracks in thick beams with a cracked beam element model. *Journal of Sound and Vibration,* 385**,** 104-124.

Malveiro, J., Ribeiro, D., Sousa, C. & Calçada, R. 2018. Model updating of a dynamic model of a composite steel-concrete railway viaduct based on experimental tests. *Engineering Structures,* 164**,** 40-52.

Moaveni, B., Conte, J. P. & Hemez, F. M. 2009. Uncertainty and sensitivity analysis of damage identification results obtained using finite element model updating. *Computer-Aided Civil and Infrastructure Engineering,* 24**,** 320-334.

Nie, J. & Cai, C. S. 2003. Steel–concrete composite beams considering shear slip effects. *Journal of Structural Engineering,* 129**,** 495-506.

Oehlers, D. & Coughlan, C. 1986. The shear stiffness of stud shear connections in composite beams. *Journal of Constructional Steel Research,* 6**,** 273-284.

Oehlers, D. J., Nguyen, N. T., Ahmed, M. & Bradford, M. A. 1997. Partial interaction in composite steel and concrete beams with full shear connection. *Journal of Constructional Steel Research,* 41**,** 235-248.

Queiroz, F., Vellasco, P. & Nethercot, D. 2007. Finite element modelling of composite beams with full and partial shear connection. *Journal of Constructional Steel Research,* 63**,** 505-521.

Sadeghi, F., Yu, Y., Zhu, X. & Li, J. 2021. Damage identification of steel-concrete composite beams based on modal strain energy changes through general regression neural network. *Engineering Structures,* 244**,** 112824.

Shu, J., Zhang, Z., Gonzalez, I. & Karoumi, R. 2013. The application of a damage detection method using Artificial Neural Network and train-induced vibrations on a simplified railway bridge model. *Engineering structures,* 52**,** 408-421.

Talebinejad, I., Fischer, C. & Ansari, F. 2011. Numerical evaluation of vibration-based methods for damage assessment of cable-stayed bridges. *Computer-Aided Civil and Infrastructure Engineering,* 26**,** 239-251.

Tan, Z. X., Thambiratnam, D. P., Chan, T. H., Gordan, M. & Abdul Razak, H. 2020. Damage detection in steel-concrete composite bridge using vibration characteristics and artificial neural network. *Structure and Infrastructure Engineering,* 16, 1247-1261.

Tu, Z. & Lu, Y. 2008. FE model updating using artificial boundary conditions with genetic algorithms. *Computers & Structures,* 86, 714-727.

Wu, Y.-F., Xu, R. & Chen, W. 2007. Free vibrations of the partial-interaction composite members with axial force. *Journal of Sound and Vibration,* 299, 1074-1093.

Wu, Y., Oehlers, D. & Griffith, M. 2002. Partial-interaction analysis of composite beam/column members. *Mechanics of Structures and Machines,* 30, 309-332.

Xia, Y., Hao, H., Brownjohn, J. M. & Xia, P. Q. 2002. Damage identification of structures with uncertain frequency and mode shape data. *Earthquake engineering & structural dynamics,* 31, 1053-1066.

Xia, Y., Hao, H. & Deeks, A. J. 2007. Dynamic assessment of shear connectors in slab–girder bridges. *Engineering Structures,* 29, 1475-1486.

Xia, Y., Hao, H., Deeks, A. J. & Zhu, X. 2008. Condition assessment of shear connectors in slab-girder bridges via vibration measurements. *Journal of Bridge Engineering,* 13, 43-54.

Xu, R. & Wu, Y. 2007. Static, dynamic, and buckling analysis of partial interaction composite members using Timoshenko's beam theory. *International Journal of Mechanical Sciences,* 49, 1139-1155.

Table 1 Comparison of theoretical and numerical modal frequencies

	Mode 1	Mode 2	Mode 3	Mode 4	Mode 5
Theoretical f (Hz)	29.05	93.20	191.1	325.7	497.8
Numerical f (Hz)	28.95	92.28	187.5	315.5	474.5
Percentage difference (%)	-0.34	-0.99	-1.91	-3.13	-4.68

Table 2 Comparison of modal frequencies between selected damage scenarios and intact situation

	Mode 1	Mode 2	Mode 3	Mode 4	Mode 5	Mode 6
Intact (Hz)	28.95	92.28	187.5	315.5	474.5	661.3
Shear connectors 5,6 removed (Hz)	28.36	92.22	185.4	311.5	472.4	660.2
% change	-2.10%	-0.07%	-1.16%	-1.30%	-0.45%	-0.18%
Shear connectors 10,11 removed (Hz)	28.95	89.21	187.3	311.3	474.0	657.1
% change	-0.02%	-3.45%	-0.10%	-1.35%	-0.12%	-0.65%
Section 2 at 50% of intact stiffness (Hz)	28.77	90.78	183.2	309.2	468.7	655.3
% change	-0.64%	-1.66%	-2.37%	-2.03%	-1.25%	-0.92%
Section 5 at 50% of intact stiffness (Hz)	28.22	91.94	183.9	312.0	467.7	651.2
% change	-2.61%	-0.38%	-1.99%	-1.11%	-1.45%	-1.56%

List of figure captions

Fig. 1. Illustration of a composite beam and internal force-deformation conditions: (a) overall configuration; and (b) sectional geometry and key internal force-deformation components.

Fig. 2. Comparison of flexural rigidity distribution of a steel-concrete composite beam under different static loads.

Fig. 3. Simply supported beam under a sinusoidal distributed load.

Fig. 4. Distributions of the flexural rigidity of a composite beam under a sinusoidal distributed load for different beam lengths.

Fig. 5. Variation of $EI_{cp\text{-}n} / EI_{full}$ with increase of the mode order.

Fig. 6. FE model of the composite beam and the serial number of the shear connectors.

Fig. 7. Sinusoidal distributed load: (a) Load 1; and (b) Load 2.

Fig. 8. Deformation shapes of the composite beam under Load 1 and Load 2.

Fig. 9. Shear slip and shear slip strain distribution of the composite beam under Load 1: (a) shear slip; and (b) shear slip strain.

Fig. 10. Shear slip and shear slip strain distribution of the composite beam under Load 2: (a) shear slip; and (b) shear slip strain.

Fig. 11. Comparison of flexural rigidity distribution under Load 1 and Load 2 between numerical and theoretical results.

Fig. 12. Flexural rigidity distributions under different component beam damage scenarios.

Fig. 13. Comparison of flexural rigidity distributions under different shear connector damage scenarios.

Fig. 14. Illustration of distinctive effects of shear connector damages and component beam section damages on the first mode shape curvature: (a) shear connector damages; and (b) component beam section damages.

Fig. 15. Illustration of comparison between updated and "actual" (target) stiffness parameters for two damage cases: (a) Case 1; and (b) Case 2

Figure

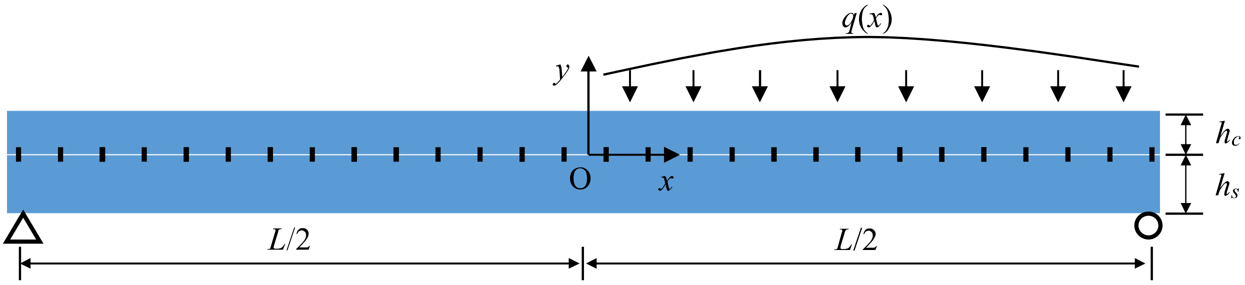

Figure

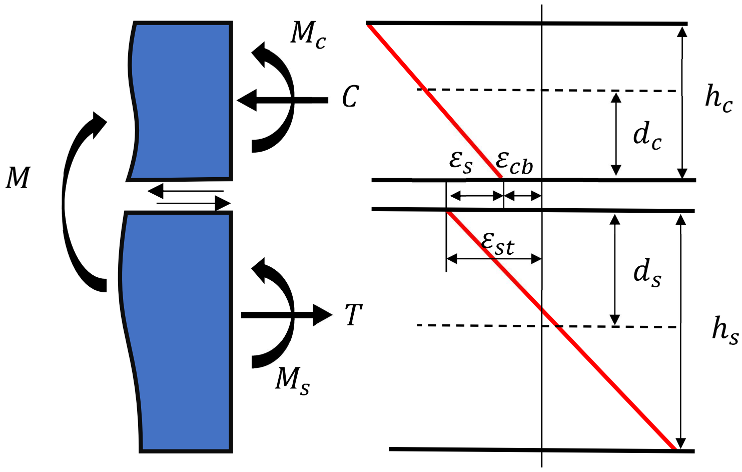

M_c
C
M
T
M_s
h_c
d_c
ε_s
ε_{cb}
ε_{st}
d_s
h_s

Figure

Click here to access/download;Figure;Fig 2.pdf

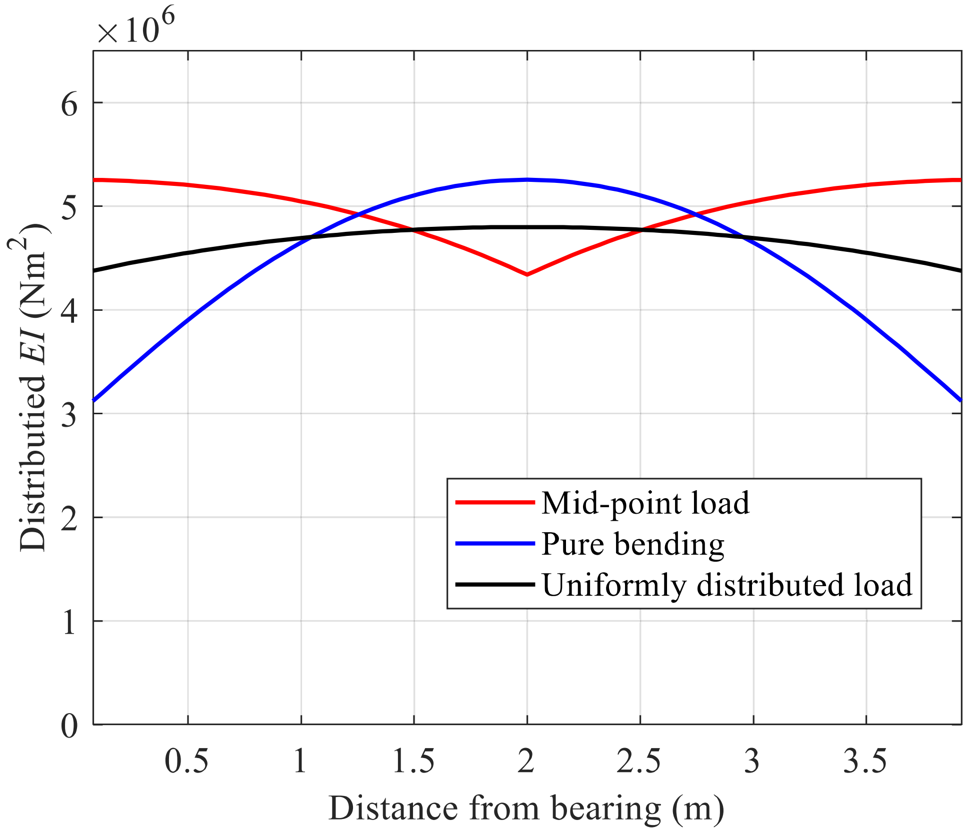

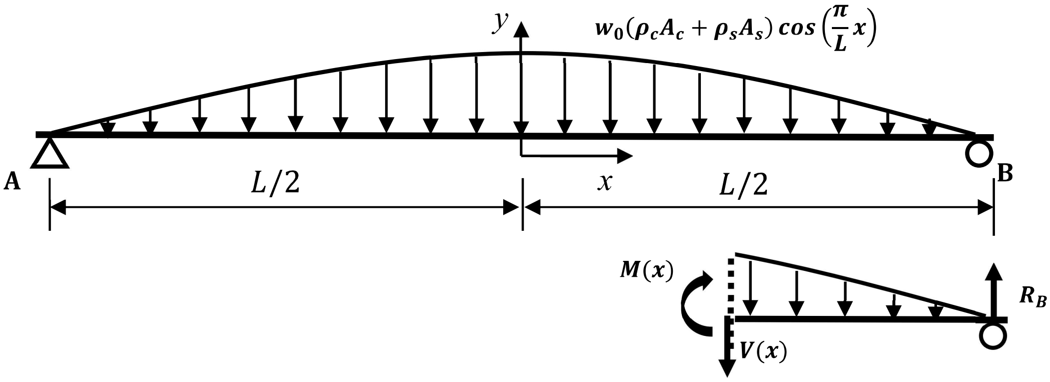
y
$w_0(\rho_c A_c + \rho_s A_s)\cos\left(\frac{\pi}{L}x\right)$
A
B
x
$L/2$
$L/2$
$M(x)$
$V(x)$
R_B

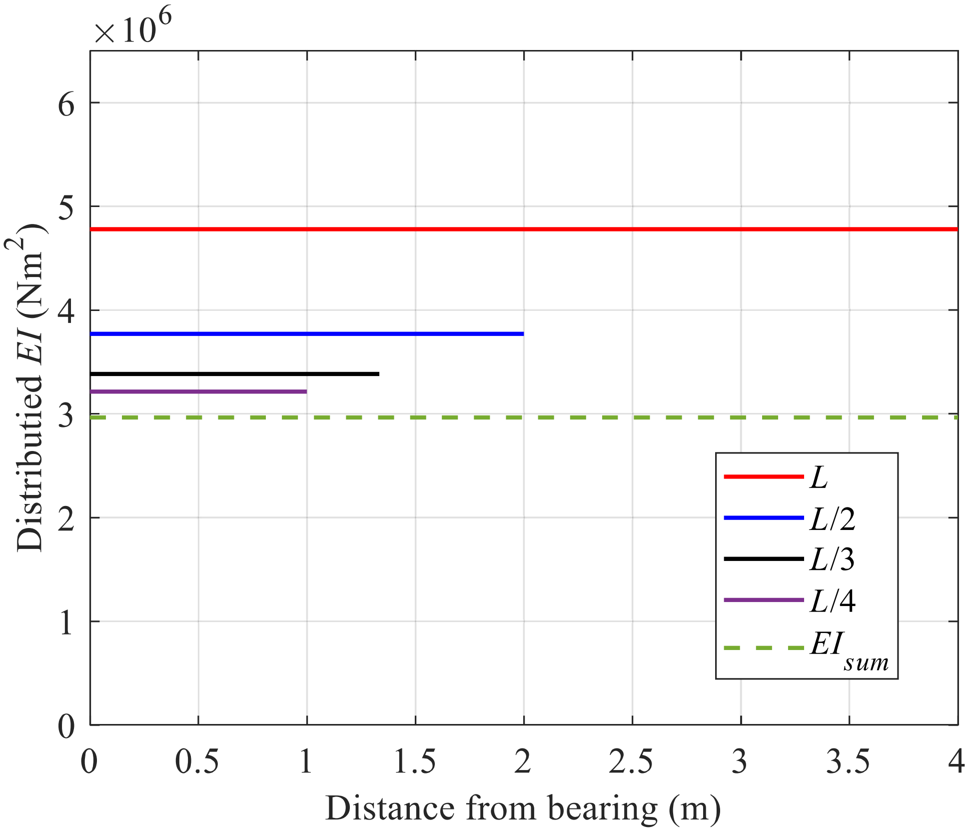
×10^6
6
5
4
3
2
1
0
Distributied EI (Nm^2)
0
0.5
1
1.5
2
2.5
3
3.5
4
Distance from bearing (m)
L
L/2
L/3
L/4
EI_sum

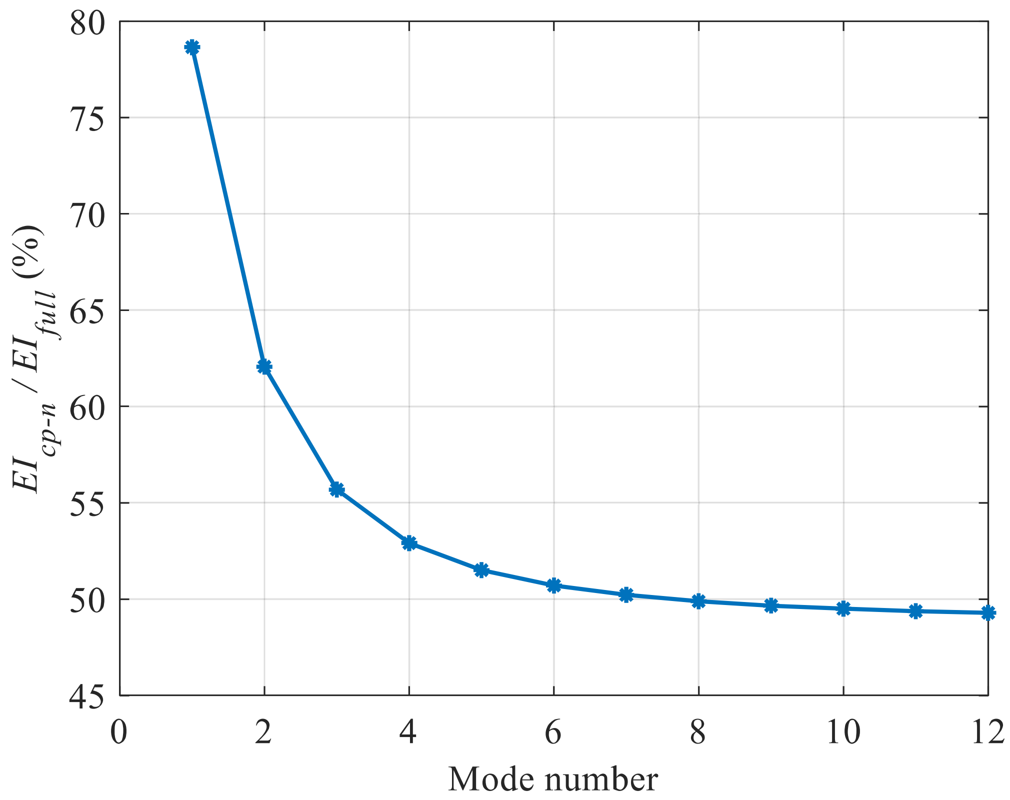
80
75
70
65
60
55
50
45
0
2
4
6
8
10
12
Mode number
EI_{cp-n} / EI_{full} (%)

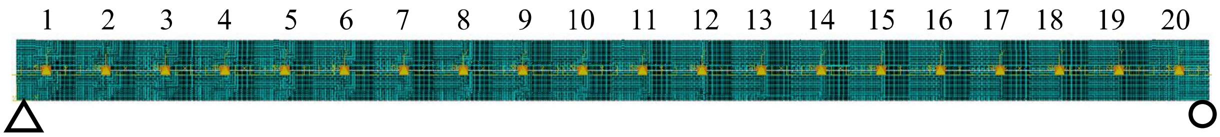
1
2
3
4
5
6
7
8
9
10
11
12
13
14
15
16
17
18
19
20

Figure

Click here to access/download;Figure;Fig 7a.pdf

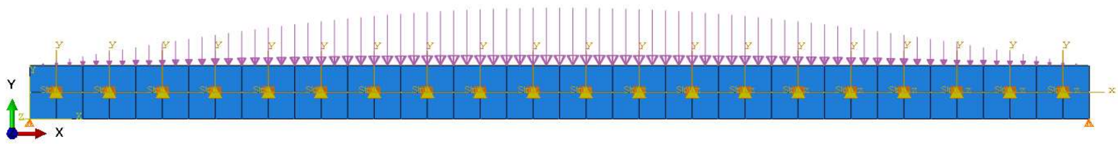

Figure

Click here to access/download;Figure;Fig 7b.pdf

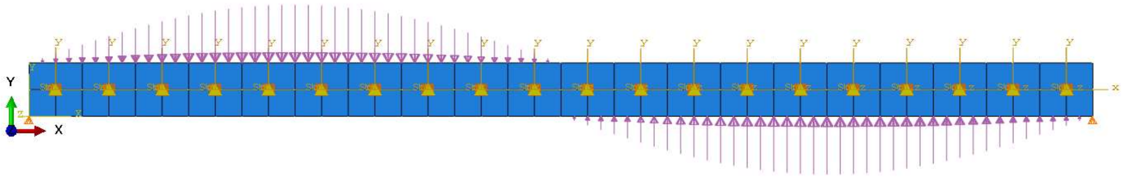

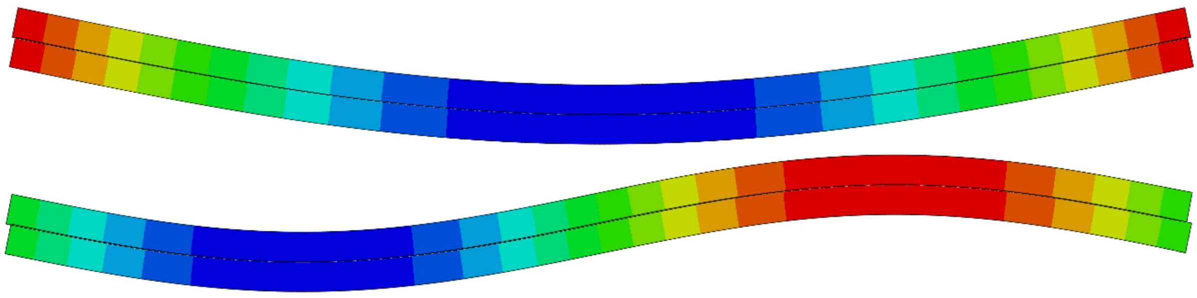

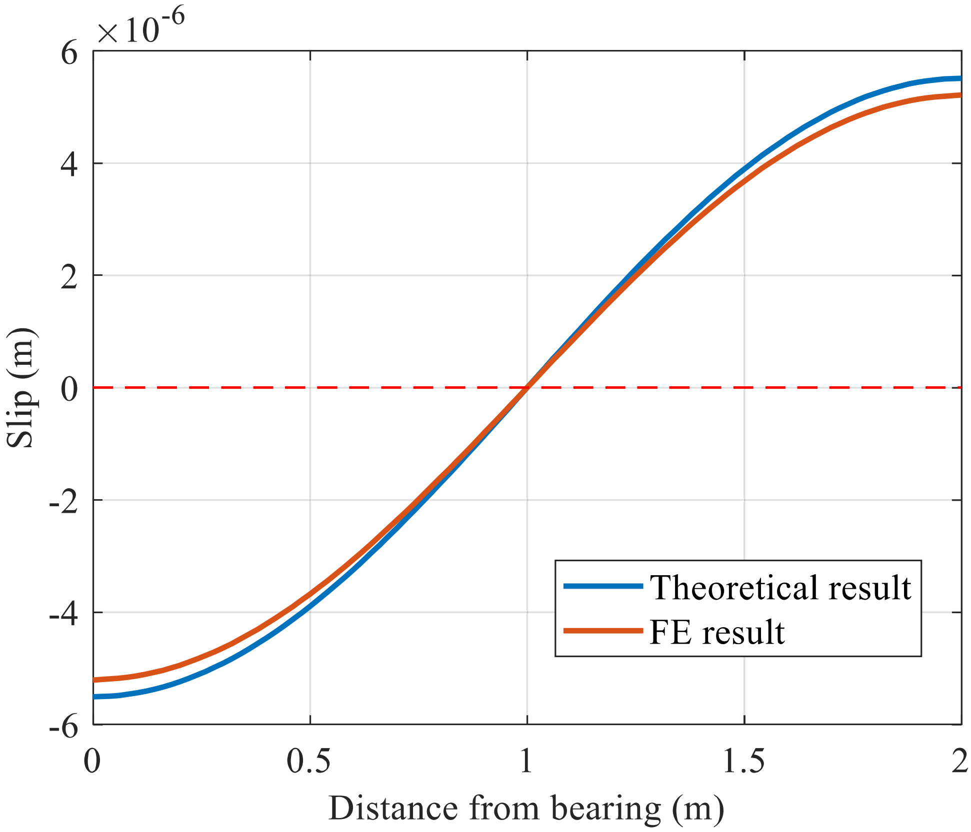
×10^-6
6
4
2
0
-2
-4
-6
Slip (m)
0
0.5
1
1.5
2
Distance from bearing (m)
Theoretical result
FE result

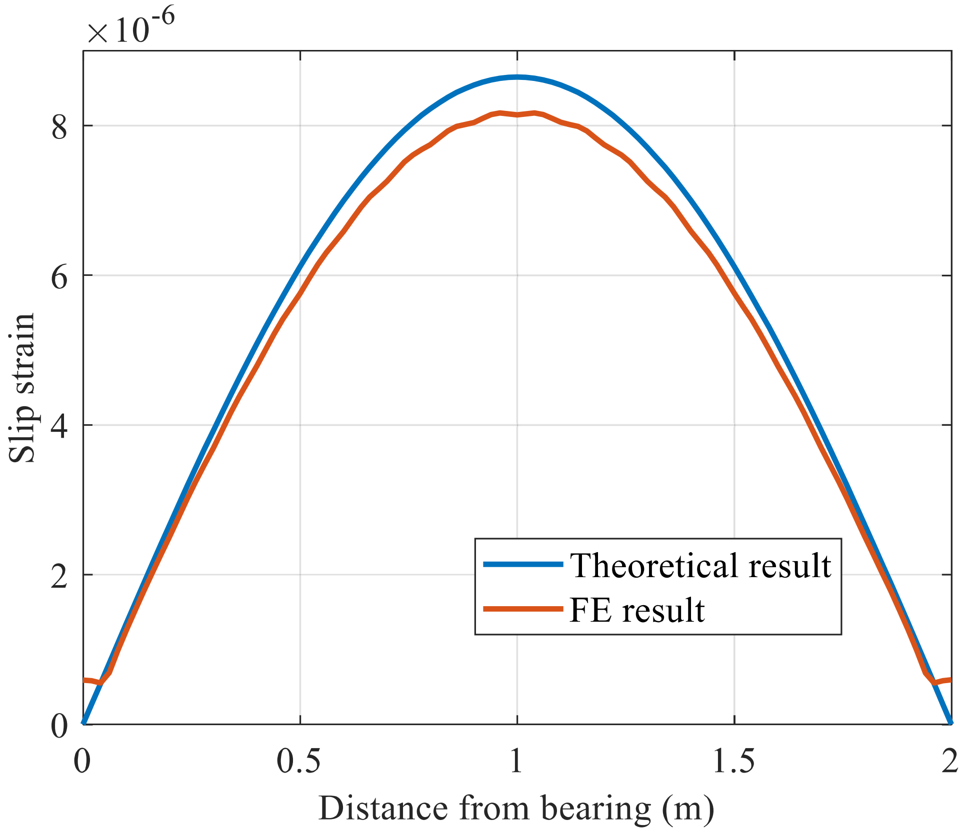
×10^-6
8
6
4
2
0
Slip strain
0
0.5
1
1.5
2
Distance from bearing (m)
Theoretical result
FE result

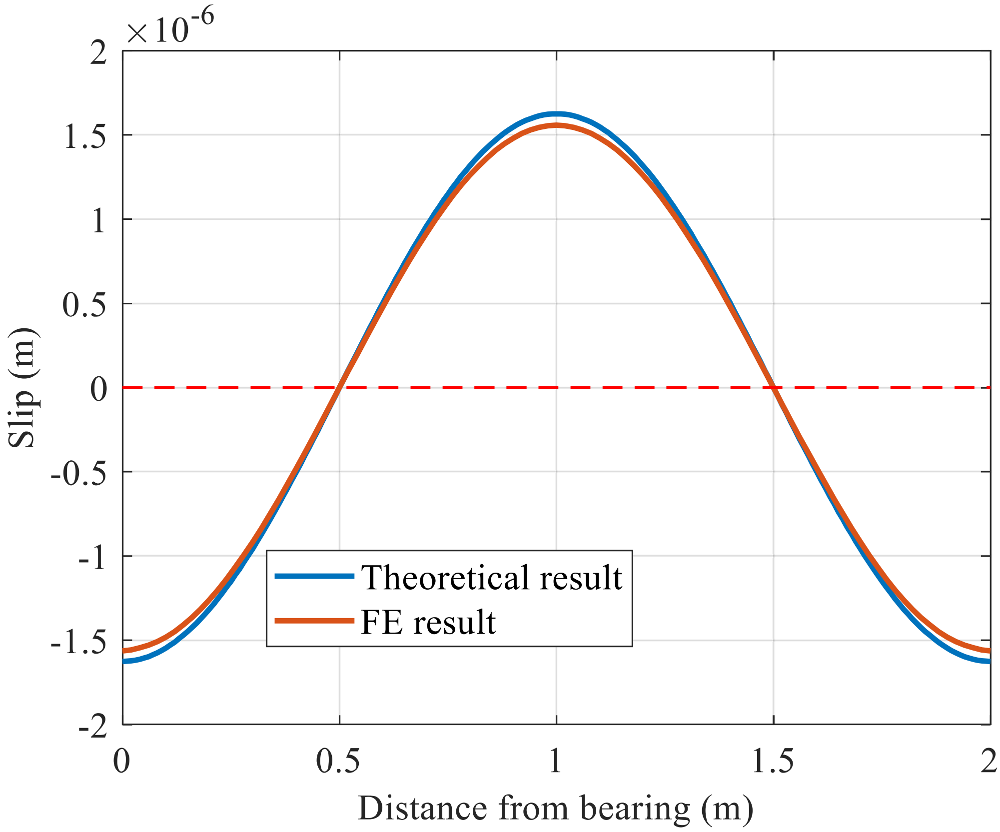
×10^-6
2
1.5
1
0.5
0
-0.5
-1
-1.5
-2
Slip (m)
0
0.5
1
1.5
2
Distance from bearing (m)
Theoretical result
FE result

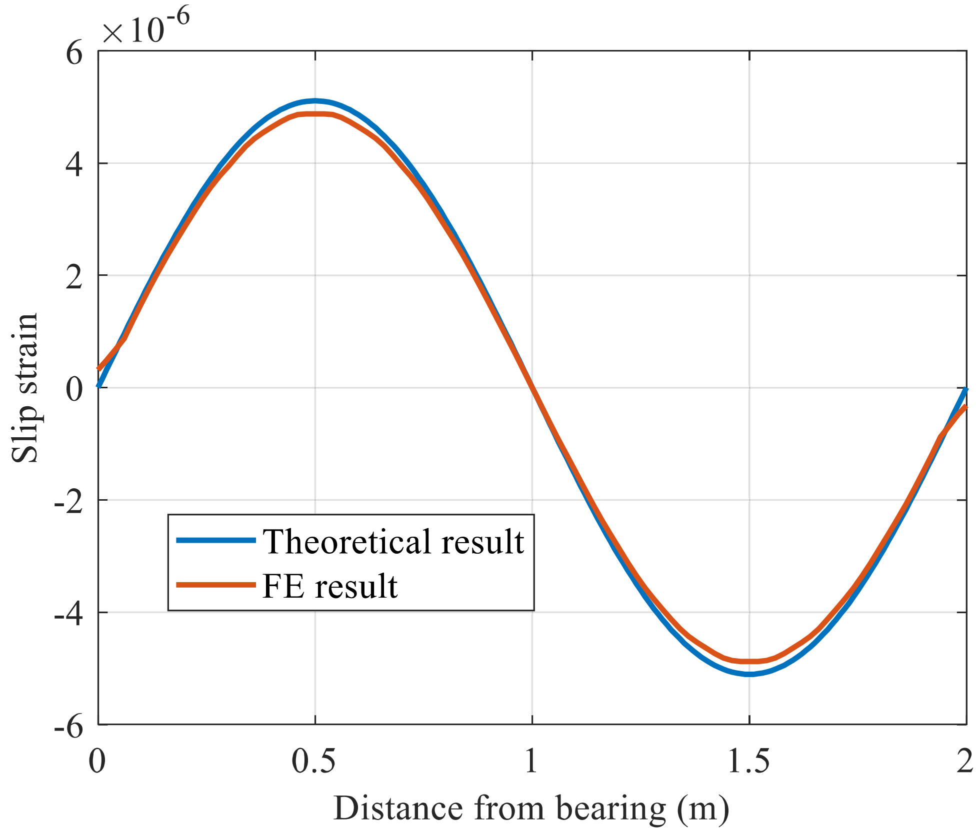
×10^-6
6
4
2
0
-2
-4
-6
Slip strain
0
0.5
1
1.5
2
Distance from bearing (m)
Theoretical result
FE result

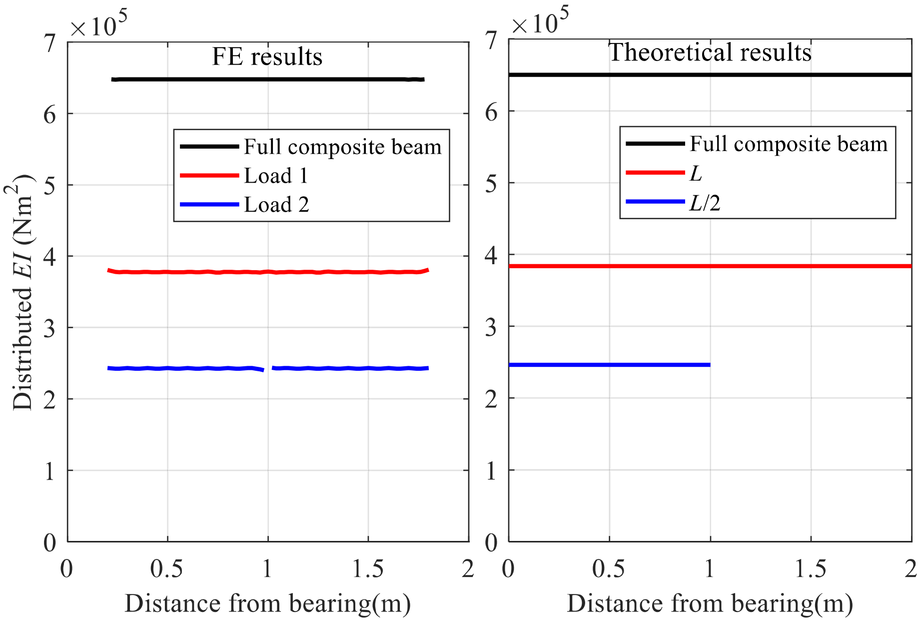
×10^5
FE results
Full composite beam
Load 1
Load 2
Distributed EI (Nm^2)
Distance from bearing(m)
0
1
2
3
4
5
6
7
0
0.5
1
1.5
2
×10^5
Theoretical results
Full composite beam
L
L/2
Distance from bearing(m)
0
1
2
3
4
5
6
7
0
0.5
1
1.5
2

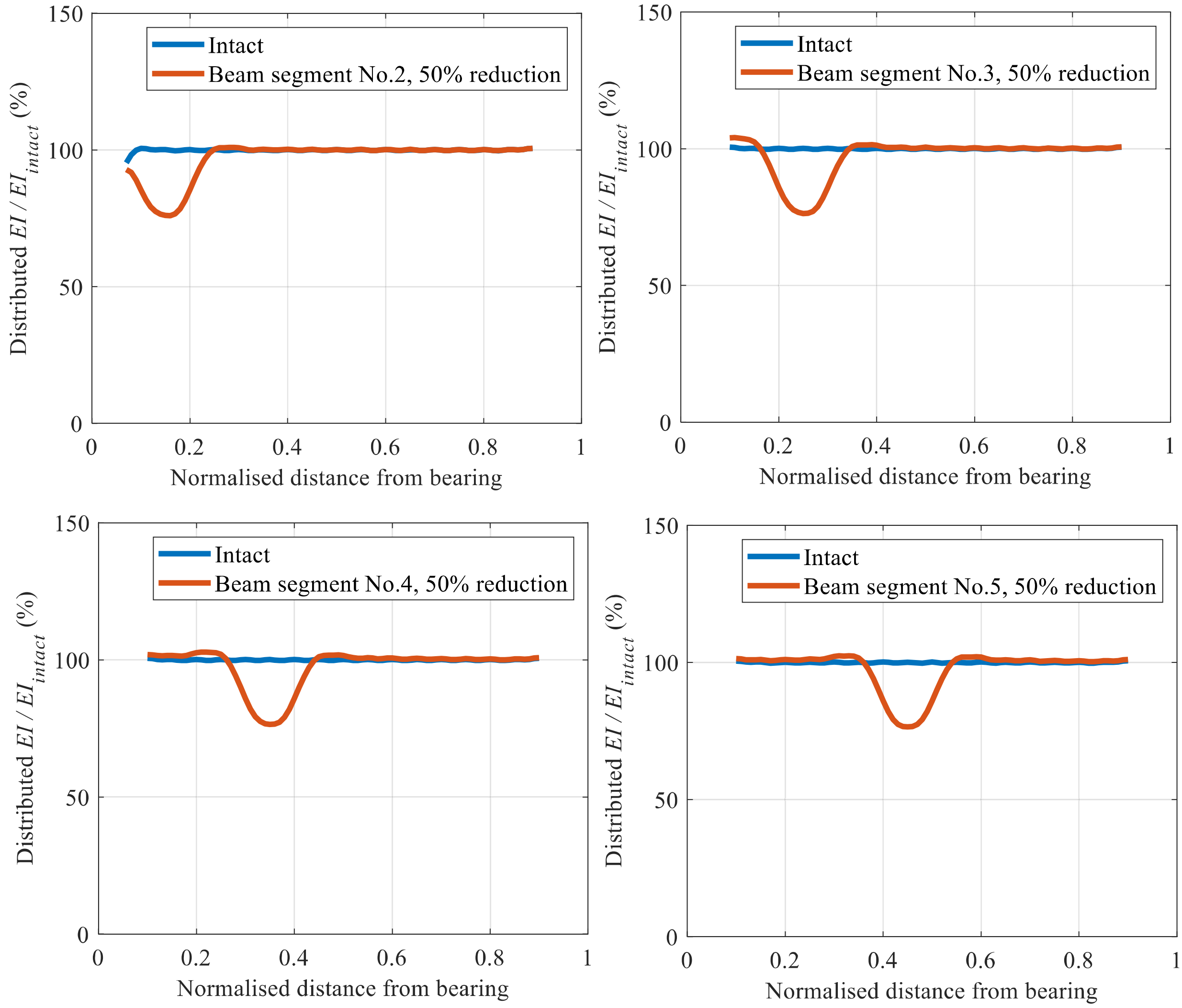
150
100
50
0
0
0.2
0.4
0.6
0.8
1
Intact
Beam segment No.2, 50% reduction
Beam segment No.3, 50% reduction
Beam segment No.4, 50% reduction
Beam segment No.5, 50% reduction
Distributed EI / EI intact (%)
Normalised distance from bearing

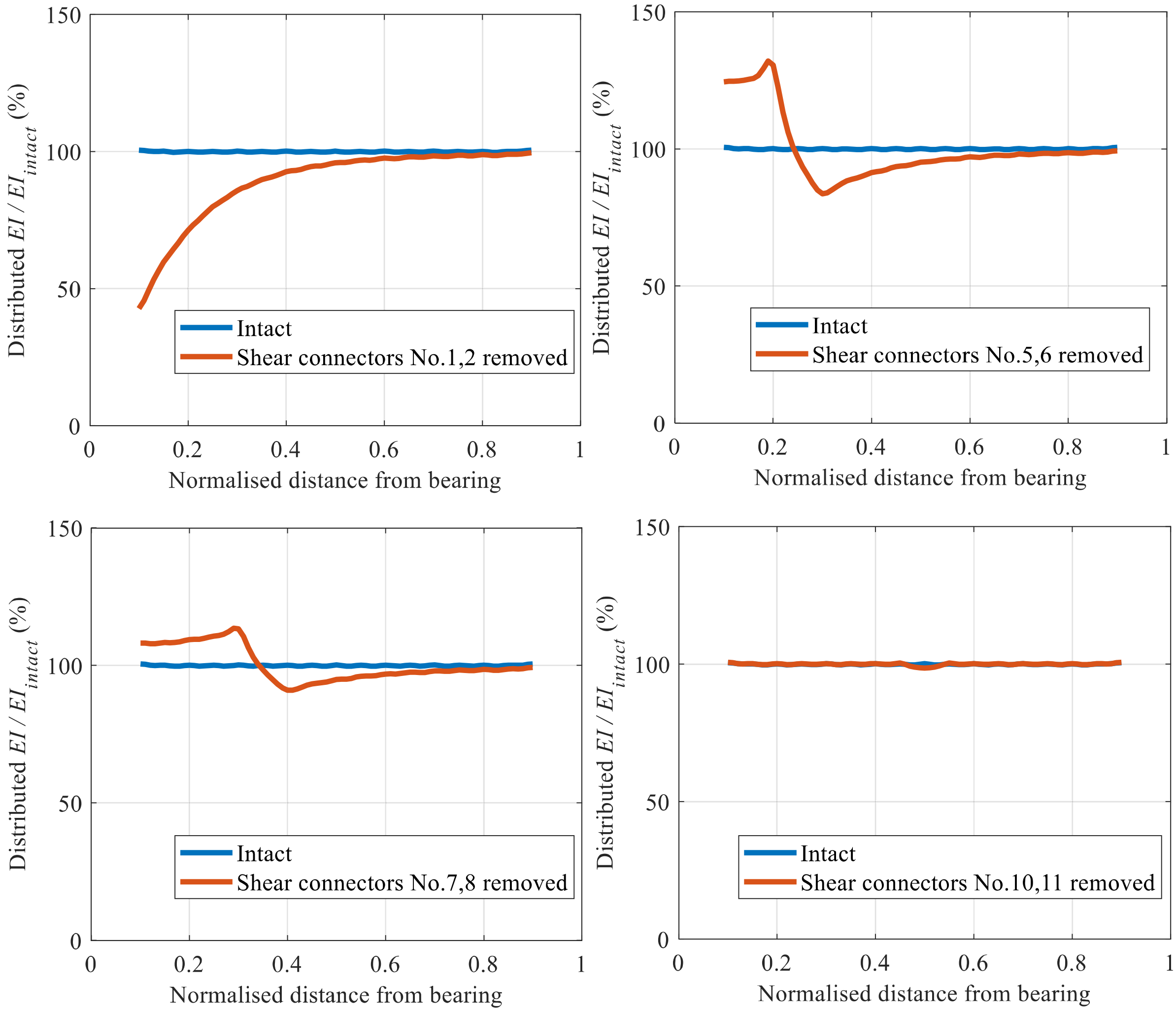
150
100
50
0
0
0.2
0.4
0.6
0.8
1
Distributed EI / EI_intact (%)
Normalised distance from bearing
Intact
Shear connectors No.1,2 removed
Shear connectors No.5,6 removed
Shear connectors No.7,8 removed
Shear connectors No.10,11 removed

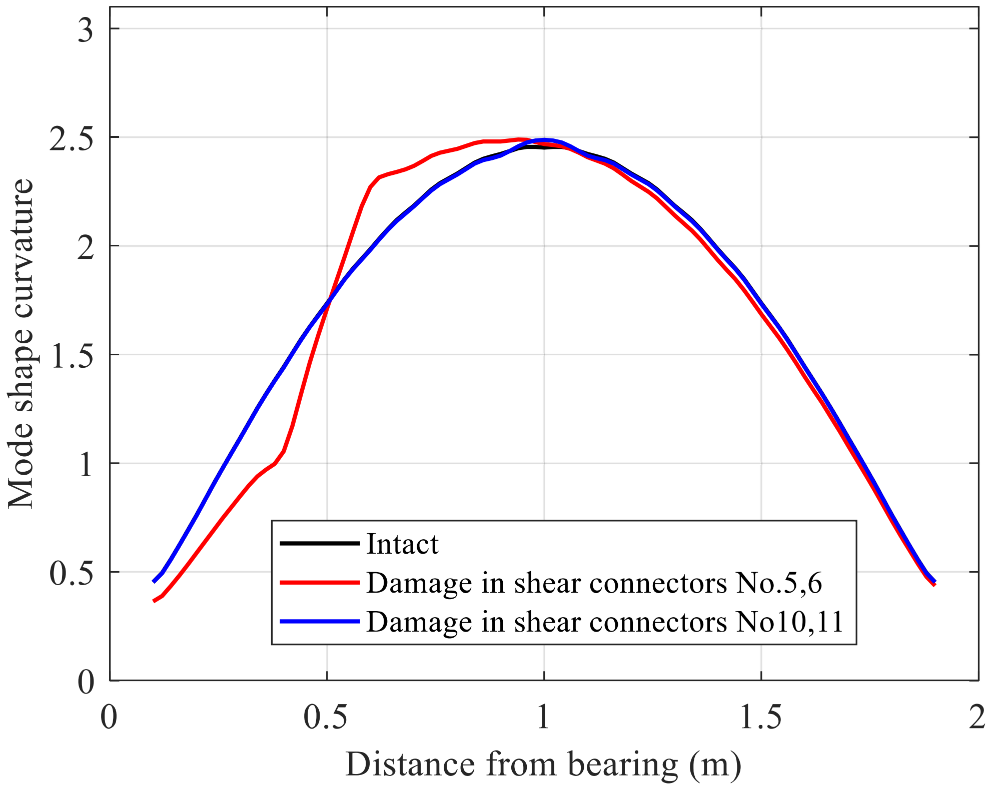
Mode shape curvature
Distance from bearing (m)
0
0.5
1
1.5
2
2.5
3
0
0.5
1
1.5
2
Intact
Damage in shear connectors No.5,6
Damage in shear connectors No10,11

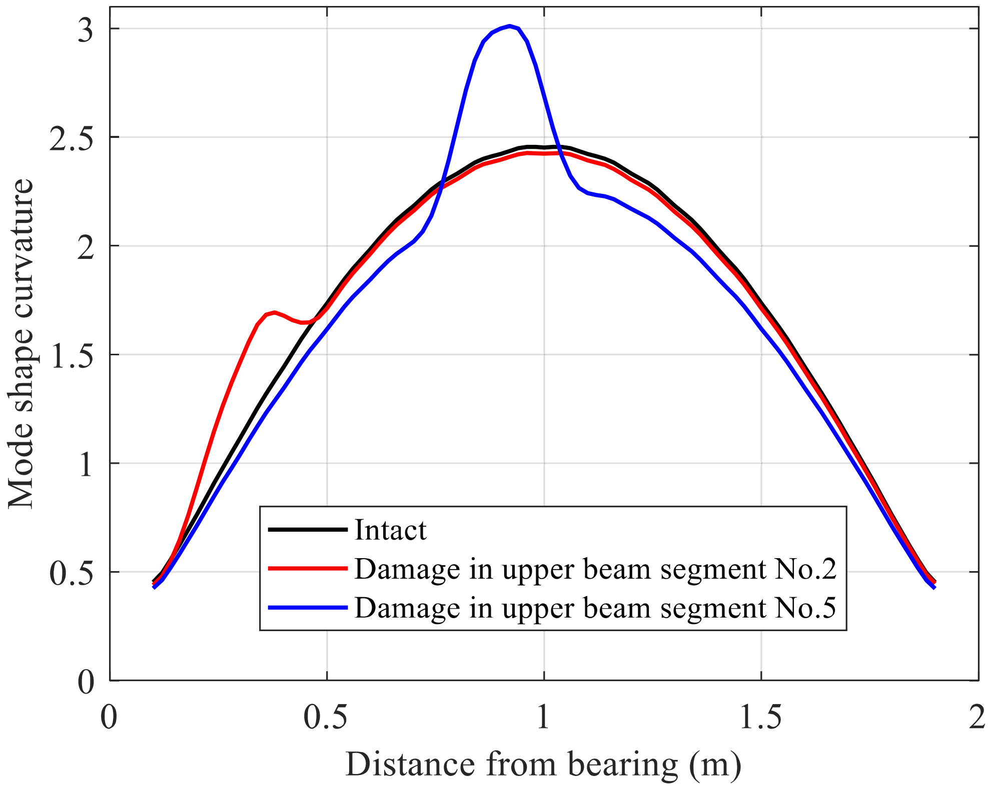
Mode shape curvature
Distance from bearing (m)
0
0.5
1
1.5
2
2.5
3
0
0.5
1
1.5
2
Intact
Damage in upper beam segment No.2
Damage in upper beam segment No.5

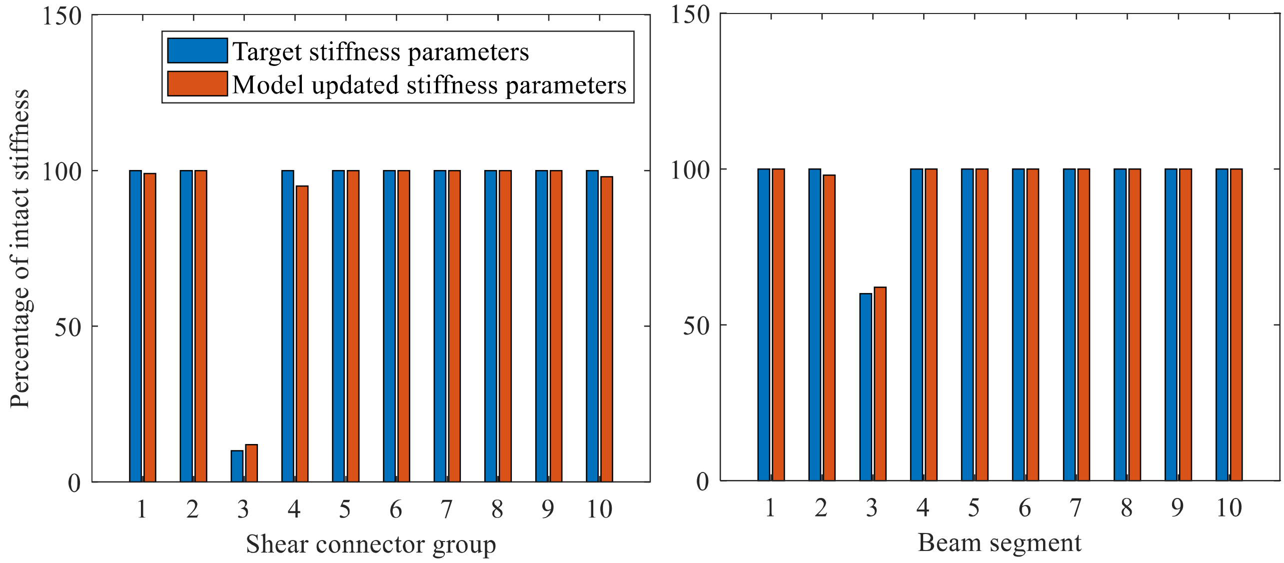
Target stiffness parameters
Model updated stiffness parameters
Percentage of intact stiffness
150
100
50
0
1 2 3 4 5 6 7 8 9 10
Shear connector group
150
100
50
0
1 2 3 4 5 6 7 8 9 10
Beam segment

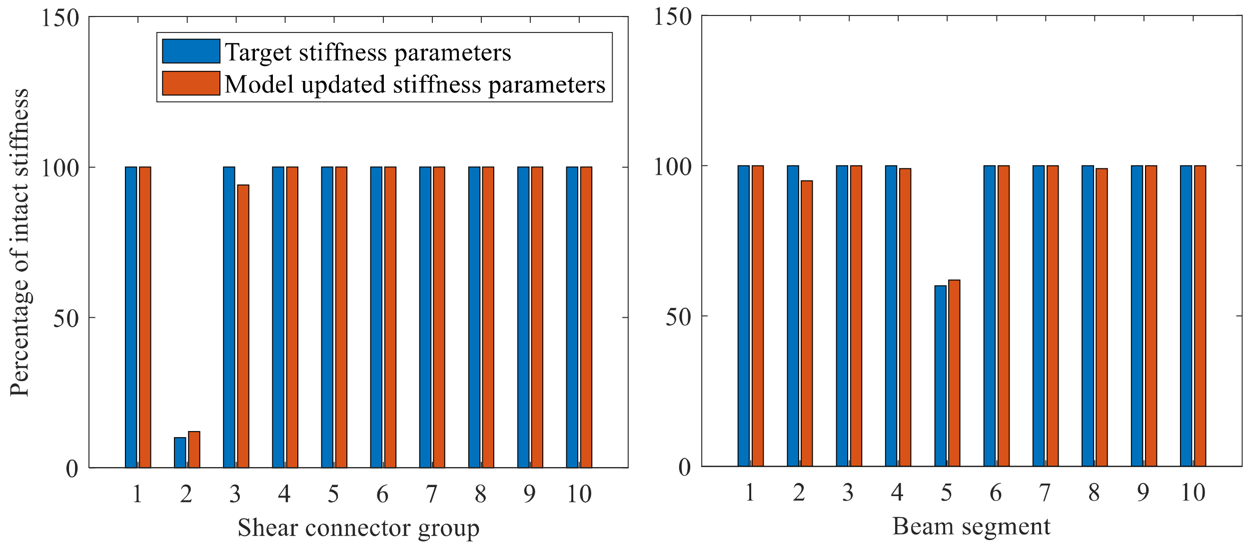
150
100
50
0
Percentage of intact stiffness
Target stiffness parameters
Model updated stiffness parameters
1
2
3
4
5
6
7
8
9
10
Shear connector group
Beam segment